

LA-UR-20-27575 (Accepted Manuscript)

Effects of Radiation-Induced Defects on Corrosion

Schmidt, Franziska
Hosemann, Peter
Scarlat, Raluca
Schreiber, Daniel
Scully, John
Uberuaga, Blas P.

Provided by the author(s) and the Los Alamos National Laboratory (2021-11-08).

To be published in: Annual Review of Materials Research

DOI to publisher's version: 10.1146/annurev-matsci-080819-123403

Permalink to record: <http://permalink.lanl.gov/object/view?what=info:lanl-repo/lareport/LA-UR-20-27575>

Disclaimer:

Los Alamos National Laboratory, an affirmative action/equal opportunity employer, is operated by Triad National Security, LLC for the National Nuclear Security Administration of U.S. Department of Energy under contract 89233218CNA000001. By approving this article, the publisher recognizes that the U.S. Government retains nonexclusive, royalty-free license to publish or reproduce the published form of this contribution, or to allow others to do so, for U.S. Government purposes. Los Alamos National Laboratory requests that the publisher identify this article as work performed under the auspices of the U.S. Department of Energy. Los Alamos National Laboratory strongly supports academic freedom and a researcher's right to publish; as an institution, however, the Laboratory does not endorse the viewpoint of a publication or guarantee its technical correctness.

1 **Title:** Effects of Radiation-Induced Defects on Corrosion

2

3 **Authors:**

4 Franziska Schmidt, franziska_schmidt@berkeley.edu, University of California Berkeley, Orcid ID:

5 <https://orcid.org/0000-0001-7537-6836>

6 Peter Hosemann, peterh@berkeley.edu, University of California Berkeley, Orcid ID:

7 <https://orcid.org/0000-0003-2281-2213>

8 Raluca O. Scarlat, scarlat@berkeley.edu, University of California Berkeley, Orcid ID:

9 <https://orcid.org/0000-0003-3302-1142>

10 Daniel K. Schreiber, daniel.schreiber@pnnl.gov, Pacific Northwest National Laboratory, Orcid

11 ID: <https://orcid.org/0000-0003-3101-5013>

12 John R. Scully, jrs8d@virginia.edu, University of Virginia, Orcid ID: [https://orcid.org/0000-0001-](https://orcid.org/0000-0001-5353-766X)

13 [5353-766X](https://orcid.org/0000-0001-5353-766X)

14 Blas P. Uberuaga, blas@lanl.gov, Los Alamos National Laboratory, Orcid ID:

15 <https://orcid.org/0000-0001-6934-6219>

16

17 **Running title:** Rad-Induced Defect Effects on Corrosion

18

19 **Corresponding authors:** Blas P. Uberuaga, blas@lanl.gov; Franziska Schmidt,

20 franziska_schmidt@berkeley.edu

21 1. Abstract

22 The next generation of nuclear reactors will expose materials to conditions that, in some cases,
23 are even more extreme than those in current fission reactors, inevitably leading to new
24 materials science challenges. Radiation-induced damage and corrosion are two key phenomena
25 that must be understood both independently and synergistically, but their interactions are
26 oftentimes convoluted. In the light water reactor community, a tremendous amount of work
27 has been done to illuminate irradiation-corrosion effects and similar efforts are underway for
28 heavy liquid metal and molten salt environments. While certain effects, such as radiolysis and
29 irradiation-assisted stress-corrosion cracking, are reasonably well-established, the basic science
30 of how irradiation-induced defects in the base material and the corrosion layer influence the
31 corrosion process still presents many unanswered questions. In this review, we summarize the
32 work that has been done to understand these coupled extremes, highlight the complex nature
33 of this problem, and identify key knowledge gaps.

34

35 **Keywords:** irradiation-corrosion, radiation effects, Gen-IV nuclear reactors, coupled extreme
36 environments, nuclear energy materials

37

38 2. Introduction

39 Materials in nuclear reactors are subjected to extreme environments encompassing radiation
40 fields, corrosive media, high temperatures and temperature gradients, and high stresses. Each
41 of these environments challenges our basic understanding of material evolution. For example,
42 radiation damage defies simple descriptions as it spans length and time scales from electrons
43 and femtoseconds to human-scale parts that evolve over decades or longer. Critically, within a
44 reactor these diverse extreme conditions impact materials simultaneously, modifying the
45 material's structure at the atomic level and its macroscopic properties. These dynamic changes
46 drive the system from thermodynamic equilibrium, establishing a critical need to understand
47 the kinetic processes underpinning material evolution. This mélange of competing kinetic and
48 thermodynamic dependencies sets the stage for critical research needed in establishing both
49 independent and interlinked factors for radiation damage and corrosion in nuclear systems.

50

51 Equilibrium and radiation-induced defects drive microstructural evolution under irradiation.
52 Solute segregation, the formation and growth of extended flaws, and enhanced surface or bulk
53 interactions follow the ebb and flow of defects throughout the microstructure. These dynamic
54 changes also strongly influence the simultaneous response of the material to the corrosive
55 coolant environment. Radiation-produced defects could alter the protectiveness of oxide layers
56 through metastable phases and enhanced diffusion kinetics. High temperature and stress can
57 further modify the properties of defect populations and their coupling to chemical species that
58 drive corrosive degradation. Thus, understanding of the coupling between irradiation and

59 corrosion begins with defects. In this review, we discuss how radiation impacts corrosion of
60 materials in contact with three nuclear coolant environments: traditional aqueous systems,
61 Lead-Bismuth Eutectic (LBE, a representative liquid metal system), and molten fluorides. After
62 introducing the basic phenomena behind both irradiation and corrosion separately, we
63 summarize past work aimed at understanding these coupled extreme environments, and close
64 by identifying outstanding specific gaps in our fundamental knowledge and subsequent
65 research directions that should be pursued.

87 3. Environments in Nuclear Systems

88 10% (2018) of global electricity is produced by 452 (2019) nuclear power reactors (1). These
89 systems expose materials to high temperature water and/or steam over decades, concurrently
90 with stress, vibration and, in the core, high neutron fluxes and temperature gradients.

91 Advanced nuclear systems may include even more extreme and exotic corrosive coolants, such
92 as reactive or Heavy Liquid Metals (HLMs), molten salts, or high temperature gases (2). It is the
93 nature of these new coolants that pose special challenges for the materials involved and our
94 understanding of those material/environment interactions. [Figure 1](#), schematically illustrates
95 the four liquid coolant reactor concepts discussed in this review.

Deleted:

96
97 The most common type of nuclear reactor is the Light Water Reactor (LWR, ~360 in operation
98 (3)), primarily in the form of Pressurized Water Reactors (PWRs) and Boiling Water Reactors
99 (BWRs). Both utilize distilled water with well-regulated chemistry as both coolant and neutron
100 moderator. In BWRs, the coolant temperature (250-350 °C) and pressures (~7 MPa) create
101 conditions where steam can be produced at 400 °C or higher. BWRs operate using high purity
102 water containing typically 0.2 mg/L (ppm) of radiolytically-produced dissolved O₂ and 20 ppb of
103 radiolytically-produced H₂ (4). Their concentration is often controlled with additives (see, e.g.,
104 (4)), as a water conductivity, representative of ionic impurities, below 0.3 μS/cm was suggested
105 to limit stress corrosion cracking (5). In the last 20 years, this has been improved to ~0.1 μS/cm
106 (5). PWRs operate with a coolant inlet temperature of 288 °C and an outlet temperature of 323 °C
107 with a pressure of 15 MPa. They utilize a hydrogen overpressure (a stoichiometric H₂ excess) and

109 a noble metal $\text{Na}_2\text{Pt}(\text{OH})_6$ chemical to maintain dissolved O_2 at less than 5 ppb (6). PWRs and
110 BWRs usually contain LiOH to control corrosion product precipitation and H_2BO_3 to control
111 nuclear reactivity. KOH is being explored as a LiOH alternative due to increasing Li demand in
112 other industries (7). The nominal pH is 7.2 in PWRs vs. 5.65 in BWRs (5). In the absence of
113 radiation effects, the chemistry variables mentioned above, along with materials factors, are
114 considered the key factors to understanding corrosion in hot water systems.

115

116 Alternative reactor technologies exist and are under active development. The sidebar
117 “Considerations in Reactor Design” discusses some of the motivations behind these new
118 technologies. Liquid metal-cooled reactors may be used where a fast neutron spectrum (> 0.5
119 MeV) is utilized for breeding or burning of fuel. While fast reactors require highly enriched fuel
120 to sustain the nuclear chain reaction, they do not need a moderator, leading to a faster neutron
121 spectrum. Numerous sodium-cooled fast reactors have been built and operated to date (8). It
122 has been found that material-coolant interactions are relatively limited in these systems as long
123 as the oxygen levels are kept low and no ternary oxides form (9). Thus, the materials
124 degradation primarily results from radiation damage from the high neutron energy and flux.
125 However, it is well known that sodium reacts with water and sodium fires have been
126 encountered in these facilities, which forms a persistent safety concern. On the other hand,
127 HLMS, such as lead or LBE, do not have this disadvantage of severe reactivity with water while
128 maintaining a fast spectrum with a reasonably low melting point ($327.5\text{ }^\circ\text{C}$ (Pb), $123.5\text{ }^\circ\text{C}$ (LBE)).
129 However, significant interactions exist between HLMS and many structural alloy species, be it
130 through the formation of intermetallic phases or dissolution into the liquid. A practical

131 limitation of LBE is that heavy metals (e.g., Bi), can breed undesirable isotopes, e.g., Po-210,
132 which reduces reactivity in the core due to its large neutron absorption cross section. The
133 synergistic effects of radiation with corrosion in these systems are mostly uncharted territory.
134
135 Molten-salt cooled reactors aim to operate at higher temperatures (700-750°C (10, 11)) than
136 LWR systems to achieve greater power conversion efficiencies. Like HLMs, the use of molten
137 salts eliminates the need for pressurized vessels and violently reactive coolants, thus attaining
138 more inherent safety features. Molten fluorides are used as a coolant in Fluoride-salt cooled
139 High-temperature Reactors (FHRs) and fluorides or chlorides act as fuel solvents and coolants in
140 Molten Salt Reactors (MSRs). FHRs utilize solid fuel pebbles that are similar to the fuel for very
141 high temperature gas-cooled reactors (12). MSRs break with the traditional solid fuel-fluid
142 coolant approach wherein the molten salt dissolves the fuel directly. Liquid fuel reduces the
143 cost of fuel production, facilitates reprocessing and recycling, and enables breed-and-burn
144 thorium fuel cycles, ultimately reducing the disposal burden (13, 14). MSRs can be designed as
145 thermal, epithermal, or fast reactors depending on the fuel and the salt used. Material
146 corrosion in molten salt is distinctly different in that protection does not rely on a passivating
147 oxide layer; instead, the importance shifts to the thermodynamic drivers for corrosion that are
148 dictated by the salt chemistry. The liquid fuel contains transmutation and fission products (FPs)
149 that represent a good fraction of the periodic table. Furthermore, the chemical species in the
150 salt can be present in transient states unique to their production from nuclear reactions and
151 the molten salt medium and reactor environment. This makes for a rich scientific challenge to

152 define and control the varied corrosion mechanisms that may arise over long-term plant
153 operation.

154

155 The described nuclear reactor concepts require materials that can withstand the co-existence
156 of corrosive environments, radiation fields, high temperatures, and, in some cases, mechanical
157 stress. These collectively represent one of the most challenging sets of operating conditions
158 imaginable.

180 4. Radiation Effects

181 Within the radiation field of the reactor core, high-energy particles emanating from nuclear
182 reactions violently interact with matter, disrupting the electronic and atomic structure of the
183 impacted materials, often with macroscale changes in material microstructure and properties.
184 While fundamental interactions – the collision of energetic particles with atoms – occur on the
185 femtosecond timescale on the length scale of atoms, macroscopic consequences can take years
186 to manifest.

187

188 The basic interactions between energetic particles and the atoms they encounter are similar
189 regardless of the state of matter, but the consequences can be very different. As schematically
190 illustrated in [Figure 2](#), depending on the mass and charge of the particles, the energetic
191 particles can interact primarily with either the electrons or the nuclei of individual atoms. In the
192 former case, irradiation by photons, electrons, and very high energy heavier particles (so-called
193 swift heavy ions with energies greater than MeV) leads predominantly to the ionization of the
194 atoms, which is embodied by electronic defects in the material. These defects can alter
195 chemical interactions that ultimately destroy the underlying crystal structure. In some ceramics,
196 swift heavy ions can directly amorphize the material along observable individual ion tracks (15–
197 18). On the other end of the spectrum, the energetic particles can displace atoms directly. The
198 extent to which this displacement happens depends on the kinetic energy of the incident
199 particle and the mass of the first atom encountered by the particle. If the kinetic energy
200 transferred to this so-called primary knock-on atom is significantly high, a collision cascade

Deleted:

224 results that can displace many thousands of atoms within a few picoseconds due to a single
225 incident particle. While most of these displaced atoms return to ordered crystallographic sites
226 (19), a fraction will remain displaced as defects – interstitials, vacancies and clusters of the
227 same – moving the system further from thermal equilibrium. The further evolution and fate of
228 these defects typically defines the net response of the solid to irradiation.

229

230 In many nuclear environments, we must also consider how irradiation interacts with the
231 corrosive medium. As fluids, liquid and gas phases both have limited internal structure and
232 respond similarly to irradiation. While atoms can be displaced, there is no long-range order to
233 be significantly altered by atomic displacement. However, irradiation can still interact with the
234 electrons that dictate bonding and, in a process called radiolysis, can disrupt that bonding,
235 forming radical species that can be more reactive with solids than the original molecules. These
236 changes to local chemistry modify the corrosive fluid and alter material corrosion as compared
237 to the bulk (unirradiated) fluid chemistry alone (20, 21). One of the simplest examples is the
238 direct disintegration of H_2O into H^+ and OH^- . Similarly, the formation of species like H_2O_2 can
239 change the oxidizing power of the electrolyte (22). The sidebar “Radiolysis in Molten Salt”
240 discusses similar potential effects in molten salts.

241

242 Turning back to solids, the damage produced during irradiation can have severe consequences
243 for the structure and ultimately the properties of the material. As highlighted in [Figure 3](#), a
244 myriad of effects are possible, including radiation-enhanced diffusion (RED), caused by the
245 super-saturation of defects responsible for atomic diffusion; radiation-induced segregation

Deleted:

247 (RIS), in which the element-specific atomic redistribution is driven by the flow of vacancies and
248 interstitials to/from microstructural sources and sinks; radiation hardening due to the
249 formation of nanoscale precipitates, dislocation loops, and voids that act as obstacles to
250 dislocations; changes in the grain structure of the material itself, either refining it as in the
251 formation of the rim structure in nuclear fuel (23) or coarsening due to enhanced kinetics; or
252 more complex aggregate effects, such as Irradiation-Assisted Stress-Corrosion Cracking (IASCC).
253 In the end, all of these radiation damage effects originate from those defects produced in the
254 incipient collision cascade.

255

256 Similarly, the extent to which radiation-induced defects can impact corrosion depends on their
257 survivability. Whether interstitials and vacancies tend to find one another and annihilate or
258 aggregate into larger defects that impact properties, depends on temperature, stress, damage
259 rate, and the fundamental nature of the material itself. As the temperature increases, the rate
260 at which defects annihilate increases, reducing their potential impact on corrosion (24).

261 However, as the damage rate increases, there is less time for defects to annihilate before new
262 defects are created. Thus, one can expect that the rate at which damage is introduced into the
263 system will be an important parameter dictating the extent to which damage impacts corrosion.

264

265 Much of the damage imparted on materials in a nuclear fission reactor is caused by high-energy
266 neutrons. While it would be ideal to study damage under realistic neutron fluxes, such
267 experiments are costly and time consuming. Materials in commercial reactors experience only a
268 few displacements per atom (dpa) per year, and even high flux reactors only achieve about 10

269 dpa per year. It is thus time-prohibitive to directly study high-exposure scenarios with this
270 approach when novel materials and reactor designs may experience hundreds of dpa over their
271 lifetime. In the case of advanced reactors, access to reactors for experimental purposes is even
272 more limited or non-existent. Further, neutrons induce transmutations and thus radioactivity
273 within materials, adding complicated and expensive radiation-safety issues to characterizing
274 neutron-irradiated samples. Surrogate irradiation environments utilizing ion beams to impart
275 damage offer an attractive alternative for fundamental studies. While having their own
276 limitations (primarily the volume of damaged material and thus the properties that can be
277 probed), ion beams can achieve exposure levels of many dpa in a day, greatly accelerating the
278 study of high-dose radiation effects. Ion beam damage, especially from light ions, such as H and
279 He, has been shown to be extremely useful in emulating neutron damage if interpreted
280 carefully (25).

281

282 5. Materials Used in Nuclear Environments

283 The varied extremes present throughout nuclear reactors necessitate careful selection of a
284 diverse range of materials depending on the performance requirements and the environment
285 of each component. The sidebar “Leak-Before-Break” discusses a less obvious selection
286 criterion applied to any nuclear reactor. For the purpose of the present discussion, we focus on
287 materials that are in contact with the corrosive medium and experience irradiation at the same
288 time. These structural materials include various steels and engineering ceramics such as SiC
289 composites.

290

291 Typical steels can be categorized as either austenitic (stainless steel) or Ferritic/Martensitic
292 (F/M). Austenitic steels contain large concentrations of Ni to stabilize the face-centered cubic
293 (fcc) phase. However, recently, other fcc-stabilized austenitic steels have gained popularity (26).
294 Activation concerns eliminate Co and other elements from the alloying toolbox. The stainless
295 steels found in LWRs include wrought and cast austenitic materials where Ni, Mn, C, and N
296 stabilize austenite at high and low temperatures.

297

298 Often, a combination of ferritic and austenitic materials is used. The body of a pressure vessel is
299 a ferritic steel (Fe-C), but its interior surfaces are lined with Corrosion Resistant Alloys (CRAs),
300 such as Ni-based alloys, Ni-Cr-Fe alloys and stainless steels. CRAs typically form a passivating
301 oxide film stable in hot water, often a Cr(III) rich oxide or hydroxide of nanometer-thickness.
302 The alloy’s Cr-content is designed to be above a critical threshold that depends on the

303 environment, but is often described as 10-14 at%, such that a continuous Cr-rich oxide may
304 form (27, 28). A bi-layered oxide is commonly formed, consisting of an Fe-rich spinel outer layer
305 over an inner layer of Cr_2O_3 or FeCr_2O_4 (27, 28).

306

307 In liquid metal systems, severe leaching of Ni can occur, limiting the use of austenitic steels in
308 LBE systems to temperatures below 550 °C. The benefit of using these materials, however, is
309 that Liquid Metal Embrittlement (LME), especially in LBE, is less of an issue while F/M materials
310 are susceptible (29). In molten salt environments, high-Ni materials are generally more
311 corrosion-resistant. It is relevant to note that, mechanically, the Ni-based systems retain
312 mechanical strength to higher temperatures than their Fe-based counterparts. However, a
313 significant disadvantage of Ni in nuclear environments is that the nuclear cross section for
314 (n, α) reactions, where a neutron is absorbed and an alpha particle or helium ion is
315 produced, is relatively high, leading to large helium buildup and significant activation concerns.
316 Void swelling is a related phenomenon in austenitic materials due to the dislocation bias for
317 point defects (30). The result of this is severe embrittlement and strength hardening under
318 irradiation in austenitic alloys.

319

320 The leaching of Ni in HLMs is a non-issue for F/M steels and the corrosion resistance is very high
321 due to Al additions (31). However, these materials do experience severe LME at 200-400 °C
322 (32). Furthermore, they are not deployed in molten salt systems because Cr is preferentially
323 attacked in molten salts (33). Finally, the tempering heat treatment of a F/M material is on the
324 order of 650 °C, limiting the operation temperature significantly.

325
326
327
328
329
330
331
332
333
334
335
336
337
338
339
340

Zirconium and Zr-based alloys are widely deployed in nuclear systems, primarily as a fuel cladding material in LWRs. The motivation for choosing Zr-based alloys is a low thermal neutron cross section paired with reasonable strength and corrosion properties. In fast reactors, a low thermal neutron cross section is not required, so liquid metal corrosion of Zr-based alloys is not widely studied. In molten salt environments, Zr-based alloys would not be suitable, as Zr is even more susceptible to attack than Cr (34). In LWR environments, Zr-based alloys form a 1-2 μm thick ZrO_2 film that is stable at standard operating conditions (35). Nuclear grade Zr-alloys often contain 1.5% Sn and other trace elements such as Hf. Zircaloy-1 containing Sn was one of the first alloys designed for cladding. Zircaloy-2 contains Sn, but also small amounts of Fe, Cr, and Ni (36). However, hydrogen adsorption during corrosion was found to be greater in alloys containing Ni (37). In Zircaloy-4, the Fe-content was raised and the Ni-content lowered to reduce hydrogen pickup. Another nuclear-grade Zr material is Zr-2.5% Nb. The presence of aliovalent cations such as Nb(III), Nb(V) and Nb(VI) is important to the oxidation resistance of Zr owing to its interaction with anions and anion vacancies.

361 6. Corrosion Effects in Nuclear Systems

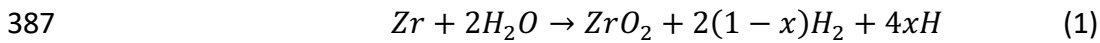
362 6.1. Water

363 Corrosion in LWR environments is typically related to high temperature oxygenated water and
364 detrimental impurities in the solution. Oxygen and oxidizers such as H_2O_2 raise electrode
365 potentials on passive metals. This provides an electrochemical driving force for local corrosion
366 where the protective oxide is broken down locally, as schematically shown in [Figure 4](#),
367 Moreover, there are many stages in localized corrosion before damage to structural materials
368 occurs, such as initiation, propagation, and arrest of the corrosion process (38). Corrosion often
369 occurs at physically occluded sites in LWRs in which the controlled bulk water chemistry is
370 altered towards more aggressive conditions that trigger corrosion. In CRAs, the defining
371 attributes are local acidification due to corrosion, metal cation hydrolysis, and O_2 depletion. To
372 maintain electroneutrality with respect to all ionic species in the hot water crevice, anions
373 congregate to balance the acidification (39). Thus, Cl^- , nitrate, or sulfate levels in crevices can
374 vastly exceed those expected in bulk LWR water chemistries. Such factors are generic across
375 many corroding systems involving hydrolysable cations such as Cr^{+3} (e.g. stainless steels and Ni-
376 based alloys). Preferential oxidation and dissolution of select alloying elements often results in
377 oxides and metal at the oxide/metal interface that are significantly altered from the bulk
378 structure and composition. We will discuss primary circuit and reactor material corrosion in the
379 absence of radiation. The secondary coolant loop is not discussed in the current review.

380

Deleted:

382 Zircaloy corrosion has been extensively studied and reviewed (40–43). As fuel cladding, this
383 material must form a thin protective oxide to retain structural integrity without compromising
384 the cladding’s heat transfer capabilities. In hot water and steam, the corrosion process is
385 characterized by uniform or nodular oxidation. The spontaneous overall corrosion reaction
386 between Zircaloy and water is (44):



388 The first hydrogen term on the right-hand side of Equation 1 represents dihydrogen gas evolved
389 upon Zr oxidation and the other represents atomic hydrogen absorbed into the Zr, where x is
390 the fractional hydrogen pickup in Zr. This reaction is thermodynamically favorable, but the
391 kinetics are governed by thick film oxidation laws which may follow limitations in growth such
392 as $\text{mass gain} = \text{constant} * (\text{time})^n$, as described by Charlesby using a Wagner-type oxidation
393 law (45), where n ranges from 0.25 to 0.5 (46) (see also sidebar “A Quick Note About Math”).
394 Oxide growth is controlled by the inward migration of O^{2-} and new oxide forms primarily at the
395 oxide/metal interface. The oxide may thicken to a critical point where residual strain eventually
396 ruptures it. At this point there may be a transition in the oxidation process where the mass gain
397 becomes linear with respect to time (47). This transition has been reported to occur at 2–3 μm
398 oxide thickness. To avoid such issues, exposure below approximately 350 °C is often
399 recommended.

400

401 Primary corrosion concerns with stainless steels in LWRs are pitting, intergranular corrosion,
402 and stress corrosion cracking. LWRs operate above critical pitting and crevice temperatures.

403 Pitting corrosion is controlled by temperature, oxidizers that raise the electrochemical driving

404 force, and the presence of impurities such as metallic species (e.g., Pb, oxidized CuCl₂) and
405 halides, particularly Cl⁻. Sulfur is also identified as a factor (48). Pits often initiate at alloy
406 inclusions (e.g. sulfides and nitrides) and defects in protective oxides. However, pitting is not a
407 major problem today given control of water chemistry (hydrogenated water, conductivity
408 below 0.1 μS/cm) and utilization of nuclear grade alloys.

409

410 Intergranular corrosion and Stress Corrosion Cracking (SCC) are historically associated with
411 sensitized grain boundaries in stainless steels and occur adjacent to intergranular chromium
412 carbides (e.g., Cr₂₃C₆ or Cr₇C₆) formed by the following solid-state reaction:



414 This reaction occurs above the solubility limit for carbon, which is about 0.03% for a Fe-18Cr-
415 8Ni alloy (49). This reaction depletes Cr from solid solution, particularly along grain boundaries,
416 to a level below the critical Cr-content for passivity. The temperature range for sensitization in
417 the austenitic stainless steel is 550-850°C. Weld heat-affected zones, for example in primary
418 coolant piping, pass through this temperature upon heating and cooling of the weld. Oxygen
419 penetration along intergranular carbides can lead to local internal oxidation, intergranular
420 cavities and shallow cracks (50).

421

422 One traditional mechanism of SCC posits that slip/film rupture occurs under dynamic plastic
423 strain where high strain and plastic strain rate ruptures the passive film to expose bare metal.
424 The bare metal subsequently repassivates by growing a new film and concurrently dissolving at
425 a rate affected by the water chemistry, oxidizer content, and the residual Cr level (51). Hence,

426 crack growth occurs by anodic dissolution and is a function of these factors, where strain and
427 strain rate play key roles. This interpretation is broadly accepted for SCC of stainless steels
428 under typical LWR conditions. An alternative theory was posited by Arioka, in particular to
429 explain SCC susceptibility of high-Cr, Ni-based alloy 690, who proposed that vacancy injection as
430 a result of surface oxidation (52) as well as the Kirkendall diffusion effect (53) create vacancies
431 clusters, voids, and eventually cavities at grain boundaries that promote further oxygen ingress
432 (54). Creep and dynamic strain are also important aspects of this argument. Cracking occurs on
433 these boundaries due to cavities affecting their strength, and cold work similarly impacts crack
434 growth rates (55).

435

436 Mitigation strategies for observed LWR corrosion issues historically have included the healing of
437 the depleted Cr, solution annealing of welds, and deployment of nuclear grade materials with
438 nitrogen and low carbon contents. For L (low C), LN (nuclear grade with N and low C) and NG
439 (low C and N) stainless steels a maximum carbon content of 0.02% is specified which is below
440 solubility limits in stainless steel (56). Moreover, 304NG and 316NG contain 0.06-0.100% N
441 which improves local corrosion resistance. However, crevices can produce the water chemistry
442 required for InterGranular SCC (IGSCC) of unsensitized stainless steel in the presence of sulfate.
443 In recent years, after low carbon was used widely, it was discovered that cracking still occurred
444 but the location of the IGSCC crack was shifted from the location of maximum Cr depletion (57)
445 to the heat affected zone near welds where sensitization is most severe (5).

446

447 Ni-base components do not typically see meaningful dose except for very specific components.
448 Alloy 600 (Ni bal, 15.5% Cr, 8% Fe, 0.08% C; wt%) and later 690 (Ni bal, 29% Cr, 9% Fe, 0.05% C
449 max; wt%) are the mainstay alloys in LWR steam generators. These alloys are also susceptible to
450 IGSCC in laboratory testing, although only alloy 600 has demonstrable IGSCC in service.
451 Thermally treated alloy 600, wherein carbide precipitation was achieved at elevated
452 temperatures to heal Cr depletion, has been broadly successful in mitigating severe IGSCC
453 susceptibility (58). Similarly, alloy 690, with ~30 wt% Cr, is largely immune to thermal
454 sensitization, intergranular corrosion or IGSCC except in extremely cold-worked material (55) or
455 under dynamic strain (59).

456

457 6.2. Liquid Metals

458 LBE has been deployed as a coolant for nuclear power applications since the 1970s, for example
459 in the OK-550 and BM-440 reactors in Soviet submarines (60). Corrosion is a well-known issue
460 in these systems and originates primarily from the solubility, and thus selective dissolution, of
461 many steel alloying elements in liquid LBE and/or the formation of intermetallic phases with Pb
462 and Bi. Although a homogeneous system would eventually saturate with dissolved species and
463 slow further dissolution, thermal gradients lead to supersaturation and precipitation of
464 dissolved species on the cold face of the heat exchanger. This can lead to clogging of pipes and
465 reduced coolant flow back to the core (see more detailed discussion in the sidebar “Failure
466 Mechanisms in HLM Systems”). To mitigate such dramatic events, oxygen is added to the LBE in
467 small quantities ($\sim 10^{-6}$ wt%) to form a passive oxide layer and prevent direct contact between
468 LBE and structural alloys. Adding too much oxygen can lead to the formation of solid PbO and

490 again can clog pipes. This approach leads to oxygen concentration guidelines as outlined in
491 [Figure 5](#), which shows the oxygen concentration regime necessary to prevent dissolution or
492 excessive oxidation. Once a passive film is established, corrosion is governed by diffusion
493 through the oxide layer. Species that have a high solubility in liquid metal, such as Ni,
494 experience a stronger driving force for diffusion than species with a lower solubility. A duplex
495 oxide layer is typically formed with an Fe-rich spinel outer layer and a Cr-rich spinel inner layer.
496 However, oftentimes sub-layers are also observed. In reference (61) it was found that the inner
497 layer contains a zone depleted of all Ni. The remnant inner oxide layer exhibited nanoscale
498 channels of interconnected porosity, especially along grain boundaries. The oxide also
499 experiences partitioning into a Cr-rich oxide and a Ni-rich phase. [Figure 6](#) shows a
500 representative oxide layer formed on a stainless steel. By contrast, Ni-free materials do not
501 experience such a dramatic dissolution process, but multiple layers are still observed. Recently,
502 Fe-Cr-Al alloys have drawn significant attention since the Al-rich oxide layer provides a better
503 passive film and a more stable diffusion barrier (31). This observation motivates the use of Al-
504 rich alloys or Al-rich weld overlay applied via various techniques on surfaces (62).
505
506 Collective experience indicates that oxidation of structural materials in LBE is faster than
507 oxidation in air, likely due to the formation of nanochannels throughout the oxide layer as
508 proposed by (63, 64). A comprehensive review of the detailed mechanisms and models
509 evaluating LBE corrosion is given by (65) and (66). However, very few tests exist above 650 °C
510 and most materials evaluated are nuclear relevant steels such as stainless steels and F/M steels.

Deleted:

Deleted:

513 Therefore, there is still much that is unknown about the fundamental mechanisms that drive
514 corrosion in these systems.
515
516 LME is another critical concern for liquid metal coolants (32). This degradation mechanism is
517 most common to F/M alloys that experience a ductility trough in the temperature range of 150-
518 400 °C (67). Austenitic materials do not experience this mechanical failure; however, they do
519 show Pb and Bi penetration along grain boundaries, associated leaching of Ni, and a subsequent
520 austenitic-to-ferritic phase transformation on a local level (68). One may speculate that
521 radiation could increase LME by enhancing diffusion and transport along grain boundaries, but
522 no in situ irradiation and corrosion tests have been carried out at relevant conditions to answer
523 this question. However, new capabilities have recently been developed (69).

524

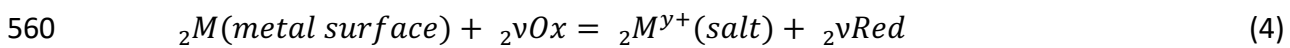
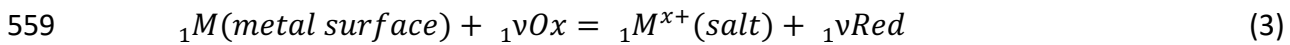
525 6.3. Molten Salts

526 In molten salts, oxide layers do not impart corrosion protection because the layers formed in
527 oxygenated molten salt environments are neither stable nor protective (33, 70) unless a
528 sufficiently high oxygen potential is present (71–73). However, such concentrations of oxygen
529 would not be compatible with liquid nuclear fuel (33) nor with graphite components. Instead,
530 the primary corrosion control in molten salts is by control of the redox potential (i.e., the
531 thermodynamic potential for corrosion). The main corrosion mechanism in molten fluorides is
532 selective removal of alloying elements via a redox reaction at the metal-salt interface. Oxidants
533 dissolved in the salt oxidize the metal to form a metal halide, which is highly soluble in the

554 molten salt and immediately dissolves. [Figure 7](#) shows representative images of corrosion
 555 effects expected in molten salt environments.

556

557 To a first order estimation, the metal halides with the most negative Gibbs free energy of
 558 formation will form preferentially over the other elements present in the metal alloy:



$$561 \quad K_1 = e^{-\frac{\Delta G_1}{RT}} = \frac{a_{{}_1M^{x+}}}{a_{{}_1M}} \cdot \left(\frac{a_{Red}}{a_{O_x}}\right)^{1\nu} \Rightarrow c_{{}_1M^{x+}} = \frac{a_{{}_1M^{x+}}}{\gamma_{{}_1M^{x+}}} = e^{-\frac{\Delta G_1}{RT}} \cdot \frac{a_{{}_1M}}{\gamma_{{}_1M^{x+}}} \cdot \left(\frac{a_{O_x}}{a_{Red}}\right)^{1\nu} \cdot \frac{O_x}{Red} \quad (5)$$

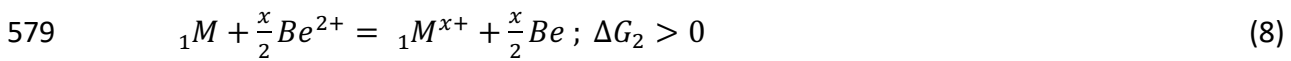
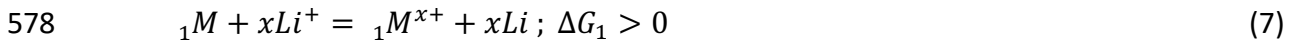
$$563 \quad \Delta G_i = \Delta G_{f, {}_iMF_x} + i\nu \Delta G_{O_x \rightarrow Red}; \text{ where } i = 1, 2$$

$$562 \quad \text{if } \Delta G_{f, {}_1MF_x} \ll \Delta G_{f, {}_2MF_y} \xrightarrow{\text{generally}} c_{{}_1MF_x(\text{salt})} > c_{{}_1MF_y(\text{salt})} \quad (6)$$

564 where ${}_1M$ and ${}_2M$ are metal species in the metal alloy in their zero-valence state and $+x$ and
 565 $+y$ oxidation states, O_x is the oxidant and Red is the product of the reduction of O_x , K is the
 566 equilibrium constant, ΔG is the Gibbs free energy of the reaction, ΔG_f is the Gibbs free energy
 567 of formation of a compound, a , γ , and c are chemical activities, activity coefficients and
 568 concentrations at equilibrium, respectively, ν are stoichiometric coefficients, T is temperature,
 569 and R is the gas constant. This preferential oxidation of one element in the alloy versus another
 570 (Equation 6) is also influenced by the surface activity of the species, $a_{{}_1M}$, and hence by its
 571 concentration and activity coefficient at the alloy/salt interface, and by the chemical activity of
 572 the corrosion product dissolved in the salt (Equation 5).

573

575 Importantly, a chemically pure, salt coolant is natively in equilibrium with metal alloys (33, 74),
576 and thus contains no driver for metal corrosion. For example, if the coolant is 2LiF-BeF₂, neither
577 LiF nor BeF₂ will reduce to oxidize any of the metal alloy components:



580 Thus, salt alone cannot corrode the metal as there is no thermodynamic driver. It is only
581 impurity oxidants or nuclear-reaction produced oxidants that can drive the preferential removal
582 of metals from the alloys; the oxidation reaction of metals necessarily requires the availability
583 of other species in the salt to reduce.

584

585 Thus, unlike their reputation to the contrary, pure molten metal halide coolants are among the
586 least corrosive media one can envision. This unearned reputation may, in part, come from the
587 absence of a passivation layer in molten salt system that is otherwise ubiquitous in oxidizing
588 corrosion systems. Additionally, the combination of ionic liquids and high temperatures results
589 in very rapid mass transport through the melt. As such, any oxidants that do come into contact
590 with and are dissolved by the salt are rapidly transported to the metal/salt interface. These
591 oxidants can dramatically alter the otherwise natively non-corrosive properties of molten metal
592 halides, and further chemistry control is needed to counterbalance these effects of oxidizing
593 solutes.

594

595 Several processes can introduce oxidants in molten salt coolants and solvents:

- 596 • Oxygen ingress, which reduces to the oxide anion O^{2-} . At low oxygen potential needed
 597 for MSR operation, the metal oxide product of this redox reaction dissolves into the
 598 molten salt.
- 599 • Water ingress provides H^+ as the oxidant and reduces to H_2 upon metal oxidation. The
 600 metal oxide and hydroxide products become soluble species in the molten salt.
- 601 • Metallic components have a native metal oxide layer upon exposure to air; thicker
 602 oxides may also be present from higher temperature processing (e.g. welding, heat
 603 treatments). These native oxides dissolve into the molten salt, introducing oxide anions
 604 O^{2-} and metal cations, some of which are oxidants to the metal alloy (e.g. Cr^{3+} , Fe^{3+} , and
 605 Ni^{2+}). This finite inventory of native oxides will deplete during operation, and
 606 consequently this driver for corrosion is eventually removed.
- 607 • Nuclear reactions are also often oxidizing processes and are further discussed below.

608

609 Lastly and very importantly, non-isothermal flow loops provide a thermodynamic driver for
 610 steady-state transport of metal. If the reaction with the oxidant is exothermic, then metals
 611 preferentially removed from the metal alloy will transport from the cold leg of the flow loop to
 612 the hot leg (75). If the reaction with the oxidant is endothermic, then alloy metals will transport
 613 from the hot leg to the cold leg (76–78). The rate of metal transport of a non-isothermal loop
 614 can be computed as:

615
$$\dot{m} \cdot [c_{1M^{x+}}(T_{hot}) - c_{1M^{x+}}(T_{cold})] = \dot{m} c_{1M^{x+}}(T_{hot}) \left(1 - e^{-\frac{\Delta H_1}{R} \left(\frac{1}{T_{cold}} - \frac{\Delta H_1}{RT_{hot}} \right)} \right) \quad (9)$$

616 where \dot{m} is the flowrate of the salt in the loop, T_{hot} and T_{cold} are the hot leg and cold leg
617 temperatures, $c_{M^{x+}}$ is the equilibrium concentration of the oxidized alloy metal, and ΔH_1 is
618 the enthalpy of the reaction of the metal with the oxidant. To minimize this transport rate, the
619 redox condition must maintain $c_{M^{x+}}$ as low as possible. Because $c_{M^{x+}}$ varies for the
620 constituents i of the metal alloy, the rate of metal transport varies with species (e.g. Cr > Ni).
621 Hence thermal gradients drive preferential removal of species from the metal alloy.

622

623 From the above considerations, preferential oxidation and subsequent dissolution of the
624 oxidation product is the dominant corrosion modality in molten halides. When the redox is not
625 well-controlled, selective loss of alloying species establishes a composition gradient at the
626 alloy/salt interface. For example, extensive Cr depletion at grain boundaries is commonly
627 observed in corrosion by molten salt, as Cr is the most susceptible major alloying element in
628 relevant structural steels and Ni-base alloys (33).

629

630 Corrosion modalities beyond redox are also possible, but have received less study. Metallic
631 tellurium, a potential FP, can lead to intergranular attack and embrittlement in Hastelloy N
632 (previously INOR-8) (79). This could be addressed by control of the redox potential of the salt to
633 prevent the formation of metallic Te. The presence of carbon in the salt can also lead to
634 carburization of the metal surface, and hence embrittlement, but also passivation, given that Cr
635 diffusion is much slower through the carburized surface layer of the metal (80). There is
636 evidence that graphite may impact the redox-type depletion of Cr, but the mechanisms for this
637 are unclear (81, 82). Lastly, because molten salt is an excellent mass transport medium, any two

638 dissimilar metal alloys in contact with a common salt will exchange elements until the
639 composition of their surfaces becomes identical to reach thermodynamic equilibrium. For
640 example, a stainless steel and a nickel surface immersed in salt can lead to transport of Cr, Fe,
641 and other alloying elements to the surface of Ni and vice versa (83). Given the complexity of
642 liquid fuel, with so many FP and activation product constituents in the salt, it is possible that
643 other corrosion modalities will be discovered in the future.
644

645 7. Simultaneous Corrosion Under Irradiation

646 Early studies on reactor-grade materials corrosion were motivated by the development of new
647 materials and unexpected component failure during operation. A short summary of a famous
648 lesson in alloy development is presented in the sidebar “Lesson Learned in Materials Design”.
649 Once the alloy design had matured, the focus shifted towards extending reactor lifetime and
650 reducing reactor downtime, both of which require a detailed understanding of why, how, and
651 how quickly corrosion progresses to reliably predict component failure. Significant progress has
652 been made in this direction for steam and water corrosion effects on steels and Ni-base alloys,
653 but the nuclear materials community faces two persistent challenges: 1) the use of new
654 materials in a corrosive environment and 2) the influence of radiation effects on components
655 and their corrosion behavior.

656

657 Initially, the impact of irradiation on corrosion was not unanimously recognized. Some studies
658 suggested minimal impact of radiation on corrosion rates (84, 85), while others showed that it
659 could drastically increase the oxidation rate of, for example, Zircaloy in water by a factor of 2
660 (86) upwards to a factor of 10 (87, 88). Evidence mounted that radiolysis was the primary cause
661 of these accelerated corrosion rates. However, other contemporary studies suggested that
662 radiation may also impact the base material and/or the corrosion layer itself (89).

663

664 Models of oxide growth in nuclear materials have changed significantly over time. A brief
665 summary given by (73) highlights the evolution from cation-mobility-based models (90) to
666 anion-mobility-based models (91) and more recent point-defect models (92). Rather than

689 focusing on cation and anion mobility, the point-defect model assumes that large
690 concentrations of anion/cation vacancies, interstitial cations, and electron-hole pairs dictate
691 the film's growth. In such a framework, it is natural to expect radiation to strongly impact these
692 defect populations and subsequent corrosion behavior of the underlying material.

693

694 Today, it is well known that radiation affects the corrosion process. Several overlapping effects
695 have to be separated experimentally, as outlined in [Figure 8](#), including the impact of radiation
696 on the material, its corrosion layer, and the corrosive medium. The corrosion process must also
697 be understood independently of radiation. In addition, corrosion under irradiation varies as a
698 function of time/age of the system, as the material, its corrosion layer, and the corrosive
699 medium evolve. In some cases, one should also consider the impact of FPs.

700

701 The complexity of the problem is challenging for experimentalists and modelers alike.
702 Fortunately, technical improvements and innovations are continually increasing our ability to
703 investigate the interactions between radiation and corrosion. The following is not an exhaustive
704 survey of all work to date in this area. Here, we focus on studies that combine simultaneous
705 irradiation and corrosion of materials and also works that separate specific effects by corroding
706 an irradiated sample or irradiating a previously corroded sample.

707

708 Aqueous corrosion studies dominate our current understanding of coupled irradiation and
709 corrosion behavior (see [Figure 9](#)). However, different coolants exhibit vastly different responses
710 dependent on the specific material and environment being considered, so understanding the

Deleted:

Deleted:

713 additional impact of radiation is nontrivial. Because of this material-coolant dependence, we
714 will present each pair of environments separately, followed by a discussion of the overarching
715 similarities and differences.

716

717 7.1.Aqueous Environments

718 7.1.1. Zircaloy – Water

719 Aqueous corrosion of Zircaloy under irradiation has been extensively studied and two of its
720 primary aspects, hydrogen uptake and IASCC, have recently been reviewed (93, 94). Previously,
721 Cox (42) summarized the known effects of irradiation on Zircaloy corrosion and provided
722 suggestions for a mechanism of radiation defect-enhanced corrosion. Several studies that
723 illuminate the relevance of environmental conditions, alloy design, and experimental design to
724 advance our understanding of where and how radiation-induced defects play a role in the
725 corrosion process are highlighted below.

726

727 Since the corrosion of Zircaloy is thought to be oxygen-diffusion limited, the availability of
728 oxygen plays a critical role. For both Zircaloy-2 and Zr-2.5%Nb, Asher et al. (88) observed a
729 strong enhancement of radiation-induced corrosion with increasing dissolved oxygen (DO)
730 content. Bradhurst et al. (95) demonstrated that the simultaneous presence of oxygen and
731 radiation is necessary to increase corrosion rates. To suppress the effects of O^{2-} production via
732 radiolysis, modern reactors operate with deoxygenated and hydrogenated water.

733

734 It was also expected that irradiation-corrosion effects would strongly depend on temperature.
735 Higher temperatures lead to temperature-accelerated diffusion kinetics, but also to increased
736 recombination rates for radiation-induced defects. Asher et al. (88) observed enhanced
737 corrosion in the presence of radiation at temperatures of 250-350 °C, but no enhancement at
738 400 °C or above where defect recombination is more prevalent. Similarly, Marlowe et al. (96)
739 reported that fuel rods experiencing lower heat flux are more susceptible to nodular corrosion,
740 indicating that temperature can also influence the type of corrosion. Shifting the temperature
741 from high (360 °C) to low (275 °C) may lead to a hysteresis effect in the oxide growth rate. For
742 example, a temperature-shifted and simultaneously irradiated Zircaloy-4 sample at first
743 resembles an unirradiated sample, as opposed to one continuously irradiated at the lower
744 temperature (97). In that study, this difference persisted for approximately 1000 days, showing
745 that radiation-induced defects in the metal or the oxide layer impact subsequent in-reactor
746 corrosion at lower temperatures.

747

748 Several mechanisms for the influence of radiation on corrosion in the Zircaloys or their oxide
749 were theorized and studied, depending on the type of energetic particle involved. These early
750 studies showed that thermal neutrons do not influence the oxidation or the hydriding process
751 of Zircaloys significantly (85). For fast neutrons, which are energetic enough to cause
752 displacement cascades, Johnson & Irvin (98) found a linear relationship between weight gains
753 and fluence (i.e., net radiation dose). They also observed that the oxidation rate varies with the
754 flux (i.e., dose rate; higher flux → more weight gain). According to (87), there appears to be a
755 saturation effect in weight gain above certain flux levels. Unfortunately, they did not determine

756 a threshold flux for their samples. (97) found that Zircaloy-4 samples exhibit flux-dependent
757 hysteresis in their corrosion rate.

758

759 Rather than by accelerating oxygen diffusion via defect production, it appears that neutrons
760 affect the corrosion rate by redistributing alloying elements, primarily Fe, from precipitates to
761 the matrix (42). The importance of precipitate size, composition, and distribution has been
762 noted in both Zircaloy-2 and Zircaloy-4 (99). Fast neutrons can induce precipitate dissolution
763 and a subsequent increase of Fe, Cr, and Ni concentrations in the matrix (100, 101).

764 Kammenzind et al. (102) recently linked accelerated corrosion rates in Zircaloy-4 to precipitate
765 dissolution, which is supported by the observation that Zr-alloys with lower or no Fe
766 concentrations or alloys where Fe is bound in more stable intermetallics show a smaller
767 acceleration of corrosion rates (42).

768

769 Fast electrons and high energy photons could impact corrosion by producing electron-hole pairs
770 and Compton electrons, increasing the conductivity of otherwise electrically insulating Zr-oxide
771 and accelerating oxygen diffusion. Radiation-induced conductivity has been shown by (103)
772 using a 1 MeV electron beam on Zircaloy-2 and Zircaloy-4. The neutron-induced dispersion of
773 Fe in the matrix may also facilitate electron motion. Localized enrichment of Fe along c-loop
774 dislocations could also result in Fe-oxide grains that act as high-conductivity paths through the
775 layer (42). More recently, (102) observed a large impact of gamma flux on Zircaloy-4. A possible
776 explanation is photon-induced oxide dissolution which has been proposed as a mechanism in
777 BWRs (104).

778

779 Many in-reactor effects are difficult to simulate in the laboratory, such as BWR nodular
780 corrosion and shadow corrosion observed on Zircaloy-2 when in proximity to other metals.
781 Both are likely galvanic processes related to the increased conductivity of the oxide layer and
782 the oxygen concentration of the water that changes the electrochemical potentials of
783 surrounding metals (42, 105).

784

785 The onset of the various effects described above varies significantly and complicates their
786 study. According to Cox (42), it appears that in-reactor radiation does not have a significant
787 effect on oxide layers less than 5 – 6 μm thick. While radiation is generally thought to affect the
788 post-transition region, there is also evidence that pre-transition corrosion can be decelerated
789 (Zr-2.5Nb (88)) or accelerated (Zircaloy-4, (106) by irradiation, requiring further study with
790 carefully designed experiments.

791

792 **7.1.1. Steel – Water**

793 Steel corrosion in aqueous reactor environments is more straightforward than for Zircalloys,
794 mainly because these components are exposed to lower temperatures, temperature gradients
795 and radiation fluxes. Studies concerned with steel corrosion for reactor environments focus
796 mainly on radiation effects on oxide layer dissolution and subsequent crud formation or IASCC.
797 Both neutron and gamma radiation can play a role in oxide modifications, either via defect
798 production or radiolysis. The radiation fields that steel components experience vary drastically
799 depending on the distance from the core. Far away, neutrons are mostly thermalized and many

800 fission gamma-rays have been absorbed. Therefore, the absorption of thermal neutrons and
801 subsequent gamma-ray production contributes more to the heating of parts and the overall
802 radiation damage than nearer the core. Consequently, one would expect different corrosion
803 behavior for steel components depending on their location due to differences in the radiation
804 fields and the thermal conditions.

805

806 There are numerous studies focusing on IASCC, which is a primary failure mechanism of
807 concern (107). IASCC is clearly influenced by both water chemistry (radiolysis) and
808 microstructure (radiation induced segregation, creep, hardening and deformation modes)
809 (107). Radiation effects in steels have been studied extensively and have been reviewed
810 recently (108–110). Because IASCC and radiolysis effects are so prevalent, few studies analyze
811 the impact of radiation damage in the metal or the oxide, or link observed effects to a single
812 source of damage. Some of these ambiguities are discussed below.

813

814 Raiman et al. (111) studied the impact of radiation-induced defects on the aqueous corrosion of
815 AISI 316L and T91 (an F/M Fe-Cr-Mo alloy) with proton irradiation. They compared oxide layers
816 grown in three different areas on the same sample: the outer unirradiated region, the center,
817 where the beam spot was located, and the “flow-region”, an area outside of the beam spot that
818 was exposed to heat and radiolysis products from the center. In 316L, the oxide layers of the
819 irradiated region and the flow-region are depleted in Cr, which does not occur in T91. This
820 suggests that Cr depletion is linked to the presence of radiolysis products and that oxides
821 formed on T91 are more resistant to radiolysis than 316L. While the oxide is thinner in the

822 beam spot than in the surrounding areas, the flow-region did not show a similar thinning,
823 indicating that either displacement damage accelerated the dissolution of the oxide or that the
824 concentration of radiolysis products in the flow-region was not high enough to cause
825 dissolution. Similar studies on 316L (112, 113) showed that both the inner and the outer layers
826 of the typical duplex oxide formed on stainless steel within the irradiated and the flow-region
827 were affected in a similar manner. However, they also studied a sample with a pre-grown oxide
828 layer in their irradiation-corrosion setup that showed porosity and Cr-depletion in the
829 irradiated zone only, indicating that radiolysis cannot be the only active process.

830

831 While increased temperatures generally promote the annealing of defects and thereby
832 decrease the impact of irradiation on steel corrosion, Kondou et al. (114) found that grain
833 boundary attack was more prominent in high-temperature (773 K) proton-pre-irradiated AISI
834 304 than for samples irradiated at lower temperatures (573 and 673 K). The authors ascribe this
835 to enhanced radiation-induced segregation at elevated temperatures.

836

837 Significantly fewer studies are available that focus on the effects of radiation on corrosion due
838 to defects introduced in the metal or oxide compared to Zircaloy, mainly because radiolysis and
839 IASCC are more prominent issues as causes of failure in steel parts. This leaves a significant gap
840 in our fundamental understanding of irradiation-corrosion effects in steels. We also note that
841 radiation effects on the corrosion of Ni-base alloys are similarly unexplored as those materials
842 are not used in significant radiation fields in LWR reactors.

843

844 7.2.Liquid Metal Environments

845 7.2.1. Steel – LBE

846 Irradiation-corrosion interactions should be simpler in heavy metal systems than in aqueous
847 environments due to a number of factors: 1) the densities of Pb and LBE are much higher than
848 that of water, removing any potential gamma radiation impact on corrosion; 2) the coolant is a
849 metal, so there is no comparable radiolysis mechanism; and 3) higher temperatures for HLM-
850 cooled designs increase the recombination rate for irradiation-induced defects and thus reduce
851 their influence on the corrosion process. Neutron-induced transmutation is, however, a bigger
852 issue for HLM systems, leading to new complications from transmutation products in the
853 corrosion process.

854

855 Relatively few LBE-cooled reactors exist, and little corrosion data are available from operational
856 or test reactors. As a result, many studies of Lead Fast Reactor (LFR) irradiation-corrosion
857 effects rely on ion accelerators to produce damage in metal samples in contact with LBE.
858 Typically, low energy protons (few MeV, e.g., the Irradiation-Corrosion Experiment (ICE) (115))
859 are chosen to simulate neutron damage. Targets for Accelerator-Driven Systems (ADS), where
860 the chain reaction is sustained by high energy protons producing neutrons from an HLM
861 spallation target, are typically studied with high energy proton beams (several hundred MeV,
862 see, e.g., the MEGAwatt Pilot Experiment (MEGAPIE) (116, 117), the DEvelopment and
863 assessment of structural materials and heavy liquid METal technologies for TRANsmutation
864 systems (DEMETRA) (118), and the GENeration IV and Transmutation Material (GETMAT) (119)
865 programs). Even fewer experiments study the impact of heavy ions (e.g., the Heavy Liquid

866 Metal and Irradiation Facility (HLMIF) (120)). A comprehensive overview of the research
867 conducted in Pb and LBE environments can be found in (121).

868

869 On the ADS side, two parts of the system may experience irradiation-corrosion related effects:
870 the core coolant system, which has challenges similar to those in LFRs, and the spallation
871 target. The MEGAPIE initiative aimed at developing an LBE spallation target with a T91 beam
872 window (122, 123). In parallel, the Liquid metal – Solid metal Reaction (LiSoR) loop (see (124))
873 studied the impact of flowing LBE on stressed steel specimens under 72 MeV proton irradiation
874 to predict the behavior of the beam window under MEGAPIE-relevant conditions (mixed
875 spectrum of 570 MeV protons and spallation neutrons). LiSoR generated several different steel
876 samples, namely T91, MANET II (a 12Cr-1Mo-Nb-V steel), and 316L, from various parts of the
877 test section that were simultaneously irradiated (< 1 dpa), corroded, and, in some cases,
878 stressed.

879

880 Several studies observed no corrosive attack on these steel samples, but found oxide layers that
881 were either thicker in the irradiated zone (> 200 hours exposure, e.g., (125, 126)) or limited to
882 that zone for short irradiation times (127). The oxides were duplex structured (Cr-rich inner
883 oxide, Fe-rich outer oxide) for both MANET II (127) and T91 samples (128). The authors
884 conclude that the differences between the irradiated and unirradiated regions are due to beam
885 heating. Gavrillov et al. (129) analyzed 316L and T91 specimens irradiated up to 9.1 dpa in the
886 BOR-60 reactor in contact with LBE (350 °C) as part of the LEXUR-II project and found no
887 evidence of corrosion attack, but evidence for a submicron oxide layer. Frazer et al. (130)

888 studied an HT-9 sample (an F/M steel) exposed to simultaneous proton irradiation (5.5 MeV, 58
889 hours) and LBE (420 °C) in the ICE setup (see (115)) and found the expected duplex oxide, which
890 had an inhomogeneous thickness across the sample. Yao et al. (120) made a similar observation
891 in SIMP steel (a martensitic steel with 10.8 wt% Cr) irradiated with a high energy 247 MeV Ar
892 beam in oxygen saturated flowing LBE (350 °C). The authors conclude that this is due to
893 irradiation damage but, unfortunately, none of these studies demonstrate conclusively whether
894 the formation of the observed oxide layers is due to elevated temperatures (beam heating) or
895 radiation effects.

896

897 Another drawback of the studies described above is that they all measure oxide thicknesses at
898 the end of the experiment, so that growth rates are averaged over its entire duration. To study
899 the corrosion rates in situ, Lillard et al. (131) used a method similar to electrical impedance
900 spectroscopy to observe the behavior of several pre-oxidized HT-9 samples irradiated with high
901 energy protons (800 MeV) in LBE (200 °C). They report a decrease in oxide impedance
902 immediately upon turning the beam on, presumably because the protons change the donor
903 density in the oxide layer. Once the beam was turned off, the impedance fluctuated widely,
904 reflecting a difficulty to repassivate. One of the samples, however, did not exhibit this
905 impedance change during irradiation or erratic behavior post irradiation. The authors conclude
906 that this indicates that there may be a potential for the optimization of the oxide's properties
907 to improve its corrosion resistance under irradiation (131).

908

909 While ion beam studies give valuable insight into certain aspects of the corrosion process, their
910 short time duration does not cover the effects of chemistry changes in a “real” system (see
911 discussion in the sidebar “Windows of Susceptibility”). Unfortunately, solubility information for
912 most of the potential spallation products in LBE or Pb do not exist (121), so their potential
913 impact on corrosion remains unclear. Recently, Hammer-Rotzler et al. (132) studied the
914 MEGAPIE and ISOLDE (133) targets and found that lanthanides tend to deposit on free metal
915 surfaces instead of remaining dissolved in the LBE. There is, however, no research specifically
916 studying their impact on the corrosion process. As noted by Dai et al. (134), the limiting factor
917 for the lifetime of a spallation target like MEGAPIE will be dominated by radiation
918 embrittlement rather than corrosion. In reactors, however, service lifetimes span several
919 decades, and the temperature tends to be higher, and thus corrosion, transmutation, and FPs
920 may be more influential and warrant further investigation at longer time scales.

921

922 7.3. Molten Salt Environments

923 For salt environments, most irradiation-corrosion studies have used molten fluoride salts due to
924 their promise as nuclear reactor coolants (see, e.g., the Molten Salt Reactor Experiment
925 (MSRE), the Molten Salt Actinide Recycler and Transmuter (MOSART), the Thorium Molten Salt
926 Reactor (TMSR), the Molten Salt Fast Reactor (MSFR), and the solid-fueled FHR (see (10, 12))).
927 Molten salt reactor designs that use molten chlorides are also pursued (see, e.g., the Molten
928 Chloride Fast Reactor (MCFR) (135)). Most studies evaluate samples irradiated in test-reactors,
929 but light ion beams are also used. Unlike aqueous and liquid metal systems, corrosion control in
930 molten salt relies heavily on the chemistry of the salt with an emphasis on redox control rather

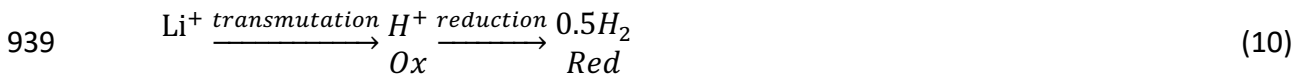
931 than formation of a passivating oxide layer. As described above, the main concern is selective
932 oxidation and dissolution of alloying elements due to the presence of oxidants in the salt.

933

934 7.3.1. Molten Fluoride-Cooled Reactors

935 When a solid fuel source is used and the molten salt is used exclusively as a coolant, chemistry
936 control is primarily focused on managing corrosion and the fate of transmutation products.

937 Specifically, Li or Be will produce tritium when transmuted, which is an oxidizing process (75,
938 136):



940

941 Different designs exist for solid fuel elements (10, 137) depending on the surrounding structural
942 materials. FHR designs use graphitic fuel elements and a graphite moderator; the presence of
943 carbon can lead to the carburization of Ni-based structural alloys (79). The effects of C in the
944 system can also lead to difficulties in the interpretation of irradiation-corrosion studies because
945 graphite crucibles are commonly used in experiments with molten salts. For example, Zheng et
946 al. (138) studied Hastelloy N and AISI 316L in Li-7 enriched FLiBe using both metal-lined and
947 graphite crucibles. Samples in graphite crucibles lost more weight than those in metal-lined
948 crucibles. In a subsequent reactor study, neutron radiation increased the weight loss compared
949 to out-of-reactor tests by factors of 10, 5, and 2 for 316L in a graphite crucible, 316L in a 316 SS-
950 lined crucible, and Hastelloy N in a Ni-lined crucible, respectively (138). Hastelloy N in the
951 graphite crucible gained weight, which the authors attribute to the possible formation of
952 carbides. The mechanism for the accelerated corrosion with neutron irradiation and in the

953 presence of carbon is not clear. In these sets of experiments the redox potential of the salts was
954 not measured or controlled. For example, for in-reactor experiments, the ingress of air,
955 moisture, and/or the production of tritium are all potential sources of oxidants that are not
956 expected with out-of-reactor experiments. These likely contribute to the observed differences
957 and more pronounced corrosion observed in the in-reactor experiments.

958

959 While irradiation is generally thought to accelerate corrosion, a recent study by Zhou et al.
960 (139) reports decelerated intergranular corrosion of Ni-20Cr in FLiNaK (0.465LiF-11.5NaF-
961 0.42KF) with added EuF_3 as oxidant (and no purification, so likely high O content),
962 simultaneously irradiated by a proton beam. Salt-filled voids formed in a Cr-depleted corrosion
963 layer and the extent and size of such voids is smaller in the irradiated region of the sample.
964 Voids are created at grain boundaries by fast grain-boundary diffusion of Cr towards the salt
965 exposed surface, while matrix diffusion of Cr and Ni to the grain boundary is more limited. The
966 authors conclude that RED and segregation promote Ni and Cr diffusion to the grain boundary,
967 which makes up for the intergranular diffusion of Cr to the sample surface, and retards void
968 formation at the attacked grain boundary. Conversely, a similar experiment with pure Fe
969 yielded the more expected result of increased corrosion in the presence of the beam,
970 attributed to a postulated effect of injected protons into the salt, although this proposed effect
971 needs further study (139).

972

973 Similarly, neutron radiation-decelerated corrosion of AISI 316L in molten NaCl-MgCl_2 was
974 reported recently by Ezell et al. (140). The authors studied samples exposed to “wet” (> 1000

975 ppm oxide) and “dry” (29 ppm oxide) NaCl-MgCl₂ with and without neutron irradiation. The
 976 sample exposed to the wet salt shows a larger corrosion depth compared to the samples
 977 exposed to the dry salt. Under neutron irradiation, the median corrosion depths of samples in
 978 both wet and dry salt are similar and smaller than in the absence of radiation, indicating that
 979 neutron irradiation decreases the depth of attack (S. Raimann, personal communication,
 980 October 20, 2020), an effect that was more pronounced for the wet salt case. The authors
 981 postulate either radiolysis effects in the salt, or a similar solid-state diffusion effect as in (139).
 982 Similar deceleration was not observed in Hastelloy N exposed to wet salt, however. In general,
 983 it is difficult to observe clear differences between the unirradiated and irradiated case at low
 984 corrosion rates,, so additional research with a larger sample size and longer exposure times are
 985 desirable (140). The results demonstrate an impact of irradiation on metal corrosion by molten
 986 salt, but also show the difficulty of decoupling irradiation effects to the material and
 987 environment from one another and from other experimental factors in irradiation-corrosion
 988 experiments.

989

990 7.3.2. Liquid-Fueled Reactors

991 In liquid-fueled MSR, another source of oxidants, uranium fission, should be considered.
 992 Fission is an oxidizing process because the summation of all FPs in their most stable oxidation
 993 state yields a valence state of +3.2 (141). Thus, the FPs originally born from U⁴⁺ will be strong
 994 oxidants:



996 Some uncertainty remains around the +3.2 value, since a good number of FPs have an uncertain
997 valence state in fluorides, due to sparse availability of thermochemical data (142). For this
998 reason, MSRs fueled with uranium will operate with a mixture of U^{3+} and U^{4+} , which acts as a
999 redox buffer that protects the alloy metals. In other words, U^{3+} is selectively oxidized before the
1000 metal alloy constituents (33). The challenge of thermal gradients nevertheless remains in
1001 convection loops, which, even in the presence of a redox buffer, lead to a continuous driver for
1002 oxidizing the metal alloy constituents. MSRE experience showed lower-than-expected corrosion
1003 for thermal loops. This effect was not explored in detail, but it was postulated to result from
1004 passivation via the deposition of noble metal fission products (Mo, Ru, Te, Nb) (79). This layer
1005 formed on both Hastelloy N and graphite (moderator) components and reached an average
1006 thickness of 10 Å (79).

1007
1008 The evaluation of samples from the MSRE also revealed a significant number of intergranular
1009 cracks on the fuel salt-facing side of the exposed Hastelloy N (143). The other side of the same
1010 part was only exposed to the FLiBe coolant and showed no cracks. Both sides exhibited the
1011 typical Cr-depleted layer, but the average corrosion depth was relatively low (79). McCoy &
1012 McNabb (143) dismissed the possibility that radiation had a direct impact because the two sides
1013 of the studied parts experienced similar temperatures and neutron fluences. Additional tests
1014 identified Te (FP) as the culprit of the intergranular attack on the fuel side. Guo et al. (144)
1015 assume that the fast diffusion of Te along grain boundaries enabled the formation of various
1016 tellurides, which in turn led to the cracks. Laboratory studies found that other alloys, such as
1017 AISI 304 and Ni- or Co-based alloys with more than 20 wt% Cr content, appear to be resistant to

1018 Te-embrittlement (143). This indicates there may be a link between Te-embrittlement and
1019 reduced Cr-content in Ni-Cr alloys, which is still an active field of research (see, e.g., (145)). The
1020 use of U^{4+}/U^{3+} can keep Te in the anionic oxidation state of -2, rather than in the metallic form,
1021 thereby mitigating Te-embrittlement (146, 147).

1022

1023 Other Ni-based alloys show very low corrosion rates in simulated reactor conditions as well.

1024 According to Ignatiev & Surenkov (148), studies on alloy HN80MT (a Ni-based alloy) have
1025 observed no effects of irradiation on corrosion in FLiBe-ThF₄-UF₄ salt, up to a power density of
1026 10 W/cm³ (temperature and time of exposure are not given). Similarly, according to Keilholtz et
1027 al. (149), early studies on Inconel (a Ni-Cr alloy) exposed in-reactor showed no observable
1028 effects of irradiation on corrosion and low corrosion rates overall with exposures of 300 hours.

1029 The authors also mention that similar measurements were performed on AISI 316, AISI 347, and
1030 Ni, and for longer exposure times, but no results are reported on these materials and the
1031 original data are not available to us. These corrosion-irradiation experiments were performed in
1032 several in-pile loops to power densities up to 800 W/cm³ and over 100 static corrosion capsules
1033 up to 8000 W/cm³, using fueled (2-27 mol% UF₄ or UF₃) salt mixtures of NaF, BeF₂, ZrF₄, and KF
1034 (spanning a range of fluoroacidity) at temperatures up to 815 °C.

1035

1036 In molten salts, the effects of fission and FPs appear to be detrimental in more than one way,
1037 but are in some cases beneficial, as discussed above. Several experiments also indicate that
1038 there is no effect of radiation on corrosion although the exposure times may not have been
1039 sufficient to draw this conclusion. In the studies where radiation-corrosion interactions were

1040 observed, it remains unclear if radiation has any direct effect on corrosion via defect production

1041 in the metal.

1063 8. Discussion and Conclusions

1064 The presented literature clearly points to the complex nature and interactions of irradiation
1065 with the corrosive behavior of materials (illustrated in [Figure 10](#)). The corrosive response
1066 depends strongly on the corrosive environment and its impurities, the chemical composition of
1067 the material, and the irradiation conditions. Because corrosion of potential reactor materials
1068 involves various processes and stages, radiation affects each and the combined effects are
1069 interdependent. At the same time, it is less clear exactly how radiation changes corrosion in
1070 many cases. Often, radiation leads to changes within the corrosive liquid; the formation of
1071 radical species can enhance the interfacial reactions that drive corrosion, and nuclear reactions
1072 are often chemical oxidizing processes. Indeed, in many of the past studies, radiolysis was a
1073 dominant effect.

1074

1075 What is less certain is the extent to which damage within the solids (base alloy or corrosion
1076 layers) changes corrosion mechanisms or rates. One would imagine that the high
1077 concentrations of defects produced during irradiation can significantly alter both solid state and
1078 liquid-mediated transport rates that drive corrosion. Further, radiation damage leads to
1079 microstructural changes, the redistribution of alloying elements, and the concomitant
1080 development of internal stresses that should also modify corrosion. Yet, as discussed by Cox
1081 (42) and more recently by Allen et al. (43), there appears to be no evidence that neutron-
1082 induced defects in the oxide layer directly enhance oxygen diffusion in Zircalloys and instead
1083 neutron-induced precipitate-dissolution appears to be dominant.

Deleted:

1107

1108 The effects of radiation-induced defects may be observed in laboratory conditions where
1109 damage rates are significantly higher (150). So, while proton damage is generally considered a
1110 good proxy for neutron damage in reactor materials (25), oxygen diffusion kinetics may not be
1111 represented accurately. This could be an issue for the interpretation of results from (mostly
1112 light) ion beam irradiation-corrosion experiments that are performed at higher damage rates
1113 than expected in-reactor (see [Figure 11](#)).

1114

1115 The extent to which these effects are important and under what conditions is still unclear. In
1116 particular, there are likely temperature and flux thresholds at which, for example, RED will
1117 impact corrosion, but these speculative thresholds are ill-defined. In the end, all of these effects
1118 are coupled. For example, phenomena such as IASCC and depletion of Cr at grain boundaries
1119 can be offset by stress relaxation due to creep deformation. A comprehensive understanding
1120 that accounts for all of these coupled effects is elusive.

1121

1122 Experiments must be designed with these coupled effects in mind to isolate the dominant
1123 effects of the studied environment. However, despite their differences, several similarities
1124 across the different environments emerge as well. Oxygen control appears to be a crucial factor
1125 regardless of reactor type. Mass transport driven by dissimilar materials has pronounced effects
1126 in molten salts and is also observed in BWRs. Such similarities could potentially be useful when
1127 exploring interactions between irradiation and corrosion that are known in one environment,
1128 but not another.

Deleted:

1130 A critical gap in our understanding of the synergies between irradiation and corrosion is
1131 highlighted by the fact that there are no models of corrosion that explicitly account for
1132 radiation damage, particularly the effect of flux and fluence, or the resulting changes in
1133 microstructure. Radiation damage clearly changes corrosion rates and mechanisms, including
1134 precipitate dissolution and redistribution of alloying elements and a memory effect in which
1135 corrosion is modified significantly by pre-existing radiation damage. Being able to predict the
1136 extent to which such effects persist is currently beyond our capabilities. Further, the
1137 experimental literature clearly points to threshold temperatures at which the effects of
1138 radiation on corrosion become minimal. Understanding exactly what dictates this critical
1139 temperature, as is done for critical pitting temperatures for conventional metal corrosion,
1140 would provide new insights for materials design. Thus, a fundamental understanding of the
1141 synergies between irradiation and corrosion is needed to better predict the performance of
1142 current materials and develop new materials for future nuclear reactor application.

1143

1144 Our review of the literature has revealed gaps in knowledge that can be summarized by these
1145 questions:

- 1146 - What is the defect content in irradiated materials and how does it influence the rates
1147 and mechanisms of corrosion? More specifically, how does this influence depend on
1148 temperature, flux, and radiation type, and at what point does the influence of the
1149 damage fade?
- 1150 - What aspects of those defects persist and impact corrosion after the radiation field is
1151 removed?

1152 - How does the solute redistribution driven by irradiation modify the way microstructure
1153 influences corrosion? How is this balanced by grain boundary migration/diffusion-
1154 induced grain boundary migration?

1155 - Ultimately, the rate of corrosion is dictated by reactions at interfaces, both solid/solid
1156 and solid/liquid. How does radiation impact these reactions and associated interfacial
1157 transport?

1158

1159 The challenge in addressing these questions relates to the complexity of the associated
1160 phenomena. Radiation damage and corrosion of materials have been studied for many decades
1161 and each represents challenging problems to materials science. These phenomena cross broad
1162 ranges of time and length scales, ultimately originating at the atomic scale but with costly
1163 macroscopic consequences. It is our view that much can be learned by simplifying the problem
1164 and choosing model systems that can both be more easily experimentally interrogated and be
1165 reasonably modeled. While certain aspects of the behavior exhibited in real engineering alloys
1166 will be missing from these systems, the salient features observed in the reactor materials
1167 should still be present. To the extent that a model system can reveal this behavior and,
1168 importantly, that behavior be predicted to some degree, we will increase our understanding of
1169 these synergies.

1170

1171 To that end, it is important to develop unique experimental and modeling capabilities to
1172 understand the synergy between irradiation and corrosion. New experimental efforts in which
1173 well-controlled and characterized samples (and well-designed control samples) are irradiated

1174 with precisely controlled particle beams provide new avenues for isolating the effects of
1175 materials damage from other effects such as beam heating, radiolysis, and changing chemistry
1176 of the corrosive medium. Similarly, new approaches to modeling corrosion that can explicitly
1177 account for all defect species within the material are critical for understanding how radiation-
1178 induced defect supersaturations impact corrosion. These steps are necessary for building a
1179 fundamental understanding of the coupled extremes of irradiation and corrosion to enable
1180 enhanced performance and safety of future reactor materials and systems.

1181

1182 **9. Acknowledgments**

1183 This work was supported as part of FUTURE (Fundamental Understanding of Transport Under
1184 Reactor Extremes), an Energy Frontier Research Center funded by the U.S. Department of
1185 Energy, Office of Science, Basic Energy Sciences. Los Alamos National Laboratory is operated by
1186 Triad National Security, LLC, for the National Nuclear Security Administration of U.S.
1187 Department of Energy (Contract No. 89233218CNA000001). Pacific Northwest National
1188 Laboratory is a multiprogram national laboratory operated by Battelle for the U.S. Department
1189 of Energy under Contract DEAC05-76RL01830.

1190 10. Literature Cited

- 1191 1. IEA. 2019. Nuclear Power in a Clean Energy System. Paris
1192 2. Allen T, Busby J, Meyer M, Petti D. 2010. Materials challenges for nuclear systems
1193 3. IAEA. 2020. Nuclear Power Reactors in the World. Vienna
1194 4. Was GS, Busby J, Andresen PL. 2006. Effect of irradiation on stress-corrosion cracking and
1195 corrosion in light water reactors. In *ASM Handbook 13C*, pp. 386–414. ASM International
1196 5. Andresen PL. 2013. Stress corrosion cracking of current structural materials in
1197 commercial nuclear power plants. *CORROSION*. 69(10):1024–38
1198 6. Hettiarachchi S, Wozadlo GP, Andresen PL, Diaz TP, Cowan RL. 1995. The concept of
1199 noble metal chemical addition technology for IGSCC mitigation of structural materials
1200 7. Demma A, Cirilli J. 2018. Primary Systems Corrosion Research Program Update
1201 8. Ohshima H, Kubo S. 2016. Sodium-cooled fast reactor. In *Handbook of Generation IV*
1202 *Nuclear Reactors*, pp. 97–118. Elsevier Inc.
1203 9. Bhatt NP, Borgstedt HU. 1988. Corrosion behaviour of structural materials in sodium
1204 influenced by formation of ternary oxides. *Mater. Corros.* 39(3):115–23
1205 10. Serp J, Allibert M, Beneš O, Delpech S, Feynberg O, et al. 2014. The molten salt reactor
1206 (MSR) in generation IV: Overview and perspectives. *Prog. Nucl. Energy*. 77:308–19
1207 11. Scarlat RO, Laufer MR, Blandford ED, Zweibaum N, Krumwiede DL, et al. 2014. Design
1208 and licensing strategies for the fluoride-salt-cooled, high-temperature reactor (FHR)
1209 technology
1210 12. Andreades C, Cisneros AT, Choi JK, Chong AYK, Fratoni M, et al. 2016. Design summary of
1211 the Mark-I pebble-bed, fluoride salt-cooled, high-temperature reactor commercial power
1212 plant. *Nucl. Technol.* 195(3):223–38
1213 13. LeBlanc D. 2010. Molten salt reactors: A new beginning for an old idea. *Nucl. Eng. Des.*
1214 240(6):1644–56
1215 14. Delpech S. 2013. Molten Salts for Nuclear Applications. In *Molten Salts Chemistry*, pp.
1216 497–520. Elsevier Inc.
1217 15. Lang M, Zhang FX, Ewing RC, Lian J, Trautmann C, Wang Z. 2009. Structural modifications
1218 of Gd₂Zr_{2-x}Ti_xO₇ pyrochlore induced by swift heavy ions: Disorder and
1219 amorphization. *J. Mater. Res.* 24(4):1322–34
1220 16. Benyagoub A. 2006. Phase transformations in oxides induced by swift heavy ions. *Nucl.*
1221 *Instruments Methods Phys. Res. Sect. B Beam Interact. with Mater. Atoms.* 245(1):225–30
1222 17. Uberuaga BP, Tang M, Jiang C, Valdez JA, Smith R, et al. 2015. Opposite correlations
1223 between cation disordering and amorphization resistance in spinels versus pyrochlores.
1224 *Nat. Commun.* 6(1):1–8
1225 18. Wang LM, Gong WL, Wang SX, Ewing RC. 1999. Comparison of ion-beam irradiation
1226 effects in X₂YO₄ compounds. *J. Am. Ceram. Soc.* 82(12):3321–29
1227 19. Nordlund K, Zinkle SJ, Sand AE, Granberg F, Averback RS, et al. 2018. Improving atomic
1228 displacement and replacement calculations with physically realistic damage models. *Nat.*
1229 *Commun.* 9(1):1–8
1230 20. Burns WG, Moore PB. 1976. Water radiolysis and its effect upon in-reactor zircaloy

- 1231 corrosion. *Radiat. Eff.* 30(4):233–42
- 1232 21. Christensen H. 1981. Effect of water radiolysis on corrosion in nuclear reactors. *Radiat.*
1233 *Phys. Chem.* 18(1–2):147–58
- 1234 22. Joseph JM, Choi BS, Yakabuskie P, Wren JC. 2008. A combined experimental and model
1235 analysis on the effect of pH and O₂(aq) on γ -radiolytically produced H₂ and H₂O₂.
1236 *Radiat. Phys. Chem.* 77(9):1009–20
- 1237 23. Une K, Hirai M, Nogita KAA, Hosokawa T, Suzawa Y, et al. 2000. Rim structure formation
1238 and high burnup fuel behavior of large-grained UO₂ fuels. *J. Nucl. Mater.* 278(1):54–63
- 1239 24. Was GS, Busby JT, Allen T, Kenik EA, Jensson A, et al. 2002. Emulation of neutron
1240 irradiation effects with protons: Validation of principle. *J. Nucl. Mater.* 300(2–3):198–216
- 1241 25. Was GS. 2015. Challenges to the use of ion irradiation for emulating reactor irradiation. *J.*
1242 *Mater. Res.* 30(9):1158–82
- 1243 26. Piatti G, Schiller P. 1986. Thermal and mechanical properties of the Cr-Mn-(Ni-free)
1244 austenitic steels for fusion reactor applications. *J. Nucl. Mater.* 141–143(PART 1):417–26
- 1245 27. Uhlig HH, Woodside GE. 1953. Anodic Polarization of Passive and Non-passive
1246 Chromium-Iron Alloys. *J. Phys. Chem.* 57(3):280–83
- 1247 28. Kirchheim R, Heine B, Fischmeister H, Hofmann S, Knotte H, Stolz U. 1989. The passivity of
1248 iron-chromium alloys. *Corros. Sci.* 29(7):899–917
- 1249 29. Proriot Serre I, Vogt JB. 2020. Liquid metal embrittlement sensitivity of the T91 steel in
1250 lead, in bismuth and in lead-bismuth eutectic. *J. Nucl. Mater.* 531:152021
- 1251 30. Zinkle SJ, Maziasz PJ, Stoller RE. 1993. Dose dependence of the microstructural evolution
1252 in neutron-irradiated austenitic stainless steel. *J. Nucl. Mater.* 206(2–3):266–86
- 1253 31. Jianu A, Fetzer R, Weisenburger A, Doyle S, Bruns M, et al. 2016. Stability domain of
1254 alumina thermally grown on Fe-Cr-Al-based model alloys and modified surface layers
1255 exposed to oxygen-containing molten Pb. *J. Nucl. Mater.* 470:68–75
- 1256 32. Kolman DG. 2019. A review of recent advances in the understanding of liquid metal
1257 embrittlement
- 1258 33. Baes CF. 1974. The chemistry and thermodynamics of molten salt reactor fuels. *J. Nucl.*
1259 *Mater.* 51(1):149–62
- 1260 34. Baes, Jr. CF. 1969. Chemistry and Thermodynamics of Molten Salt Reactor Fuels. *Nucl.*
1261 *Metall.* 15:617–44
- 1262 35. Jin G, Xu C, Hu S, Zhou X. 2020. Temperature dependent electrochemical equilibrium
1263 diagram of zirconium-water system studied with density functional theory and
1264 experimental thermodynamic data. *J. Nucl. Mater.* 532:152036
- 1265 36. Yau TL, Webster RT. 1983. Effects of Iron on the Corrosion Resistance of Zirconium.
1266 *Corrosion.* 39(6):218–26
- 1267 37. Yau TL, Webster RT. 1995. Delayed hydride cracking of zirconium alloys
- 1268 38. Scully JR. 2019. Future frontiers in corrosion science and engineering, Part II: Managing
1269 the many stages of corrosion. *Corrosion.* 75(2):123–25
- 1270 39. Galvele JR. 1976. Transport Processes and the Mechanism of Pitting of Metals. *J.*
1271 *Electrochem. Soc.* 123(4):464–74
- 1272 40. Cox B. 1968. Effects of irradiation on the oxidation of zirconium alloys in high
1273 temperature aqueous environments. A review
- 1274 41. International Atomic Energy Agency. 1998. Waterside Corrosion of Zirconium Alloys in

- 1275 Nuclear Power Plants. *IAEA-TECDOC*
- 1276 42. Cox B. 2005. Some thoughts on the mechanisms of in-reactor corrosion of zirconium
1277 alloys
- 1278 43. Allen TR, Konings RJM, Motta AT, Couet A. 2020. Corrosion of Zirconium Alloys. In
1279 *Comprehensive Nuclear Materials - 2nd Edition*, ed RJM Konings, R Stoller. Elsevier
- 1280 44. Machiels AJ. 1987. Corrosion of Zircaloy-Clad LWR Fuel Rods: Corrosion in High
1281 Temperature Water. In *Metals Handbook 9th addition*, p. 946. ASM International. Vol. 13
1282 ed.
- 1283 45. Wagner C. 1952. Theoretical Analysis of the Diffusion Processes Determining the
1284 Oxidation Rate of Alloys. *J. Electrochem. Soc.* 99(10):369
- 1285 46. Charlesby A. 1953. Ionic currents in thin films of zirconium oxide. *Acta Metall.* 1(3):340–
1286 47
- 1287 47. Bradhurst DH, Heuer PM. 1970. The influence of oxide stress on the breakaway oxidation
1288 of zircaloy-2. *J. Nucl. Mater.* 37(1):35–47
- 1289 48. Park JR, Szklarska-Smialowska Z. 1985. Pitting Corrosion of Inconel 600 in High-
1290 Temperature Water Containing CuCl₂. *Corrosion.* 41(11):665–75
- 1291 49. Davidson RM, DeBold T, Johnson MJ. 1987. No Title. In *Metals Handbook 9th addition*, p.
1292 547. ASM International. Vol. 13 ed.
- 1293 50. Zhai Z, Toloczko M, Kruska K, Bruemmer S. 2017. Precursor evolution and stress
1294 corrosion cracking initiation of cold-worked alloy 690 in simulated pressurized water
1295 reactor primary water. *Corrosion.* 73(10):1224–36
- 1296 51. Ford FP. 1996. Quantitative Prediction of Environmentally Assisted Cracking. *Corros.*
1297 52(5):375–95
- 1298 52. Desgranges C, Lequien F, Aublant E, Nastar M, Monceau D. 2013. Depletion and voids
1299 formation in the substrate during high temperature oxidation of Ni-Cr alloys. *Oxid. Met.*
1300 79(1–2):93–105
- 1301 53. Kirkendall E. 1939. Rates of diffusion of copper and zinc in alpha brass
- 1302 54. Arioka K. 2020. Role of cavity formation on long-term stress corrosion cracking initiation:
1303 A review. *Corrosion.* 76(2):142–75
- 1304 55. Toloczko MB, Olszta MJ, Bruemmer SM. 2011. One Dimensional Cold Rolling Effects on
1305 Stress Corrosion Crack Growth in Alloy 690 Tubing and Plate Materials
- 1306 56. Sedriks AJ. 1996. *Corrosion of stainless steels, 2nd Edition*. Wiley
- 1307 57. Gordon BM, Gordon GM. 1987. No Title. In *Metals Handbook 9th addition*, p. 927. ASM
1308 International. Vol. 13 ed.
- 1309 58. Féron D, Guerre C, Herms E, Laghoutaris P. 2016. Stress corrosion cracking of alloy 600:
1310 Overviews and experimental techniques. In *Stress Corrosion Cracking of Nickel Based*
1311 *Alloys in Water-Cooled Nuclear Reactors: The Coriou Effect*, ed D Féron, RW Staehle, pp.
1312 325–53. Elsevier Inc.
- 1313 59. Moss T, Kuang W, Was GS. 2018. Stress corrosion crack initiation in Alloy 690 in high
1314 temperature water. *Curr. Opin. Solid State Mater. Sci.* 22(1):16–25
- 1315 60. Kim TK. 2013. GEN-IV Reactors. In *Nuclear Energy*, ed N Tsoulfanidis, pp. 175–201. New
1316 York: Springer
- 1317 61. Hosemann P, Dickerson R, Dickerson P, Li N, Maloy SA. 2013. Transmission electron
1318 microscopy (TEM) on oxide layers formed on D9 stainless steel in lead bismuth eutectic

- 1319 (LBE). *Corros. Sci.* 66:196–202
- 1320 62. Heinzl A, Kondo M, Takahashi M. 2006. Corrosion of steels with surface treatment and
1321 Al-alloying by GESA exposed in lead-bismuth. *J. Nucl. Mater.* 350(3):264–70
- 1322 63. Martinelli L, Balbaud-Célérier F, Terlain A, Delpech S, Santarini G, et al. 2008. Oxidation
1323 mechanism of a Fe-9Cr-1Mo steel by liquid Pb-Bi eutectic alloy (Part I). *Corros. Sci.*
1324 50(9):2523–36
- 1325 64. Martinelli L, Balbaud-Célérier F, Picard G, Santarini G. 2008. Oxidation mechanism of a
1326 Fe-9Cr-1Mo steel by liquid Pb-Bi eutectic alloy (Part III). *Corros. Sci.* 50(9):2549–59
- 1327 65. Zhang J, Li N. 2008. Review of the studies on fundamental issues in LBE corrosion. *J. Nucl.*
1328 *Mater.* 373(1–3):351–77
- 1329 66. Zhang J, Hosemann P, Maloy S. 2010. Models of liquid metal corrosion
- 1330 67. Van den Bosch J, Hosemann P, Almazouzi A, Maloy SA. 2010. Liquid metal embrittlement
1331 of silicon enriched steel for nuclear applications. *J. Nucl. Mater.* 398(1–3):116–21
- 1332 68. Hosemann P, Frazer D, Stergar E, Lambrinou K. 2016. Twin boundary-accelerated
1333 ferritization of austenitic stainless steels in liquid lead-bismuth eutectic. *Scr. Mater.*
1334 118:37–40
- 1335 69. Rossi F, Fumagalli F, Ruiz-Moreno A, Moilanen P, Hähner P. 2020. Membrane bulge test
1336 rig for irradiation-assisted stress-corrosion cracking. *Nucl. Instruments Methods Phys.*
1337 *Res. Sect. B Beam Interact. with Mater. Atoms.* 479:80–92
- 1338 70. Raiman SS, Lee S. 2018. Aggregation and data analysis of corrosion studies in molten
1339 chloride and fluoride salts. *J. Nucl. Mater.* 511:523–35
- 1340 71. Nishimura H, Terai T, Yamawaki M, Tanaka S, Sagara A, Motojima O. 2002. Compatibility
1341 of ferritic steels with Li₂BeF₄ molten salt breeder. *J. Nucl. Mater.* 307–311(Part 2):1355–
1342 59
- 1343 72. Terai T, Hosoya Y, Tanaka S, Sagara A, Motojima O. 1998. Compatibility of structural
1344 materials with Li₂BeF₄ molten salt breeder. *J. Nucl. Mater.* 258–263(Part 1):513–18
- 1345 73. Tzvetkoff T, Kolchakov J. 2004. Mechanism of growth, composition and structure of oxide
1346 films formed on ferrous alloys in molten salt electrolytes - A review. *Mater. Chem. Phys.*
1347 87(1):201–11
- 1348 74. Olander D. 2002. Redox condition in molten fluoride salts: Definition and control. *J. Nucl.*
1349 *Mater.* 300(2–3):270–72
- 1350 75. Stempien JD, Ballinger RG, Forsberg CW. 2016. An integrated model of tritium transport
1351 and corrosion in Fluoride Salt-Cooled High-Temperature Reactors (FHRs) – Part I: Theory
1352 and benchmarking. *Nucl. Eng. Des.* 310:258–72
- 1353 76. McNeese LE. 1976. Molten-Salt Reactor Program -- Semiannual Progress Report for
1354 Period Ending February 29, 1976. Oak Ridge
- 1355 77. Ignatiev V, Surenkov A. 2012. Material performance in molten salts. In *Comprehensive*
1356 *Nuclear Materials.* 5:221–50. Elsevier Ltd
- 1357 78. Ignatiev V, Surenkov A. 2017. Corrosion phenomena induced by molten salts in
1358 Generation IV nuclear reactors. In *Structural Materials for Generation IV Nuclear*
1359 *Reactors*, pp. 153–89. Elsevier Inc.
- 1360 79. Haubenreich PN, Engel JR. 1970. Experience with the Molten-Salt Reactor Experiment.
1361 *Nucl. Appl. Technol.* 8(2):118–36
- 1362 80. Chan KJ, Ambrecht RJ, Luong JM, Choi WT, Singh PM. 2018. Carburization effects on the

- 1363 corrosion of Cr, Fe, Ni, W, and Mo in fluoride-salt cooled high temperature reactor (FHR)
 1364 coolant. *Ann. Nucl. Energy*. 120:279–85
- 1365 81. Qiu J, Wu A, Li Y, Xu Y, Scarlat R, Macdonald DD. 2020. Galvanic corrosion of Type 316L
 1366 stainless steel and Graphite in molten fluoride salt. *Corros. Sci.* 170:108677
- 1367 82. Zheng G, Kelleher B, Cao G, Anderson M, Allen T, Sridharan K. 2015. Corrosion of 316
 1368 stainless steel in high temperature molten Li₂BeF₄ (FLiBe) salt. *J. Nucl. Mater.* 461:143–
 1369 50
- 1370 83. Falconer C, Doniger WH, Bailly-Salins L, Buxton E, Elbakhshwan M, et al. 2020. Non-
 1371 Galvanic Mass Transport in Molten Fluoride Salt Isothermal Corrosion Cells. *Corros. Sci.*,
 1372 p. 108955
- 1373 84. Eichenberg JD, Lieberman RM, Mrazik FP. 1960. Irradiation of UO₂ Fuel Rods - The XII
 1374 Experiment. *WAPD-208*, April
- 1375 85. Dalgaard SB. 1962. Corrosion and hydriding behaviour of some Zr 2.5 wt% Nb alloys in
 1376 water, steam and various gases at high temperature. Chalk River, Ontario, Canada
- 1377 86. Johnson, Jr A. 1977. Behavior of spent nuclear fuel in water pool storage. Richland, WA
 1378 (United States)
- 1379 87. Burns W, Maffei H. 1962. Neutron Irradiation and Cold Work Effects on Zircaloy-2
 1380 Corrosion and Hydrogen Pickup. In *Corrosion of Zirconium Alloys*, pp. 101–17. West
 1381 Conshohocken, PA: ASTM International
- 1382 88. Asher RC, Davies D, Kirstein TBA, McCullen PAJ, White JF. 1970. The effects of radiation
 1383 on the corrosion of some Zr alloys. *Corros. Sci.* 10(10):695–707
- 1384 89. Jenks GH. 1961. *Review and correlation of in-pile zircaloy-2 corrosion data and a model
 1385 for the effect of irradiation*. Oak Ridge National Laboratory
- 1386 90. Cabrera N, Mott NF. 1949. Theory of the oxidation of metals. *Reports Prog. Phys.*
 1387 12(1):163–84
- 1388 91. Fehlner FP, Mott NF. 1970. Low-temperature oxidation. *Oxid. Met.* 2(1):59–99
- 1389 92. Chao CY, Lin LF, Macdonald DD. 1981. A Point Defect Model for Anodic Passive Films: I.
 1390 Film growth kinetics. *J. Electrochem. Soc.* 128(6):1187
- 1391 93. Suman S, Khan MK, Pathak M, Singh RN, Chakravartty JK. 2015. Hydrogen in Zircaloy:
 1392 Mechanism and its impacts
- 1393 94. Was GS, Andresen PL. 2012. Irradiation assisted corrosion and stress corrosion cracking
 1394 (IAC/IASCC) in nuclear reactor systems and components. In *Nuclear Corrosion Science
 1395 and Engineering*, pp. 131–85. Elsevier Ltd
- 1396 95. Bradhurst DH, Shirvington PJ, Heuer PM. 1973. The effects of radiation and oxygen on
 1397 the aqueous oxidation of zirconium and its alloys at 290 °C. *J. Nucl. Mater.* 46(1):53–76
- 1398 96. Marlowe MO. 1985. Nuclear fuel cladding localized corrosion
- 1399 97. Hillner E, Franklin DG, Smee JD. 2000. Long-term corrosion of Zircaloy before and after
 1400 irradiation. *J. Nucl. Mater.* 278(2):334–45
- 1401 98. Johnson ABJ, Irvin JE. 1967. Radiation-enhanced oxidation of Zircaloy-2 in pH-10 LiOH
 1402 and pH-10 NH₄OH. Pacific Northwest Laboratory, Richland, WA (United States)
- 1403 99. Cheng B, Adamson RB. 1987. Mechanistic studies of Zircaloy nodular corrosion
- 1404 100. Etoh Y, Shimada S. 1992. Irradiation-Induced Dissolution of Precipitates in Zircaloy-2. *J.
 1405 Nucl. Sci. Technol.* 29(4):353–66
- 1406 101. Kruger RM, Adamson RB. 1993. Precipitate behavior in zirconium-based alloys in BWRs. *J.*

- 1407 *Nucl. Mater.* 205:242–50
- 1408 102. Kammenzind BF, Gruber JA, Bajaj R, Smee JD. 2018. Neutron irradiation effects on the
1409 corrosion of zircaloy-4 in a pressurized water reactor environment
- 1410 103. Howlader MMR, Kinoshita C, Shiiyama K, Kutsuwada M, Inagaki M. 1999. In situ
1411 measurement of electrical conductivity of Zircaloy oxides and their formation mechanism
1412 under electron irradiation. *J. Nucl. Mater.* 265(1–2):100–107
- 1413 104. Kritsky VG, Petrik NG, Berezina IG, Doilnitsina Vni Piet V V. 1993. Effect of Water
1414 Chemistry and Fuel Operation Parameters on Zr + 1% Nb Cladding Corrosion
- 1415 105. Lysell G, Nystrand A-C, Ullberg M. 2005. Shadow Corrosion Mechanism of Zircaloy
- 1416 106. Wang P, Was GS. 2015. Oxidation of Zircaloy-4 during in situ proton irradiation and
1417 corrosion in PWR primary water. *J. Mater. Res.* 30(9):1335–48
- 1418 107. Was GS, Andresen PL. 2007. Stress corrosion cracking behavior of alloys in aggressive
1419 nuclear reactor core environments
- 1420 108. Andresen PL, Was GS. 2019. Irradiation Assisted Stress Corrosion Cracking. In
1421 *Comprehensive Nuclear Materials*, pp. 190–217. Elsevier
- 1422 109. Chopra OK, Rao AS. 2011. A review of irradiation effects on LWR core internal materials -
1423 IASCC susceptibility and crack growth rates of austenitic stainless steels. *J. Nucl. Mater.*
1424 409(3):235–56
- 1425 110. Garner FA. 2020. Radiation-Induced Damage in Austenitic Structural Steels Used in
1426 Nuclear Reactors. In *Comprehensive Nuclear Materials - 2nd Edition*, ed RJM Konings.
1427 Elsevier
- 1428 111. Raiman SS, Wang P, Was GS. 2017. Irradiation Accelerated Corrosion of Stainless Steel
1429 and Ferritic-Martensitic Steel in Simulated Primary Water
- 1430 112. Raiman SS, Bartels DM, Was GS. 2017. Radiolysis driven changes to oxide stability during
1431 irradiation-corrosion of 316L stainless steel in high temperature water. *J. Nucl. Mater.*
1432 493:40–52
- 1433 113. Raiman SS, Was GS. 2017. Accelerated corrosion and oxide dissolution in 316L stainless
1434 steel irradiated in situ in high temperature water. *J. Nucl. Mater.* 493:207–18
- 1435 114. Kondou K, Hasegawa A, Abe K. 2004. Study on irradiation induced corrosion behavior in
1436 austenitic stainless steel using hydrogen-ion bombardment
- 1437 115. Qvist S, Bolind AM, Hosemann P, Wang Y, Tesmer J, et al. 2013. Capability demonstration
1438 of simultaneous proton beam irradiation during exposure to molten lead-bismuth
1439 eutectic for HT9 steel. *Nucl. Instruments Methods Phys. Res. Sect. A Accel. Spectrometers,*
1440 *Detect. Assoc. Equip.* 698:98–105
- 1441 116. Dai Y, Wohlmuther M, Boutellier V, Hahl S, Lagotzki A, et al. 2016. Non-destructive
1442 testing of the MEGAPIE target. *J. Nucl. Mater.* 468:221–27
- 1443 117. Saito S, Suzuki K, Hatakeyama Y, Suzuki M, Dai Y. 2020. Experimental validation of tensile
1444 properties measured with thick samples taken from MEGAPIE target. *J. Nucl. Mater.*
1445 534:152146
- 1446 118. Fazio C. 2011. Technology and Components of Accelerator-driven Systems. In *Technology*
1447 *and Components of Accelerator-driven Systems*. OECD Publishing
- 1448 119. Fazio C, Briceno DG, Rieth M, Gessi A, Henry J, Malerba L. 2011. Innovative materials for
1449 Gen IV systems and transmutation facilities: The cross-cutting research project GETMAT
- 1450 120. Yao C, Wang Z, Zhang H, Chang H, Sheng Y, et al. 2019. HLMIF, a facility for investigating

- 1451 the synergistic effect of ion-irradiation and LBE corrosion. *J. Nucl. Mater.* 523:260–67
- 1452 121. Fazio C, Sobolev VP, Aerts A, Gavrilov S, Lambrinou K, et al. 2015. Handbook on Lead-
- 1453 bismuth Eutectic Alloy and Lead Properties, Materials Compatibility, Thermal-hydraulics
- 1454 and Technologies - 2015 Edition
- 1455 122. Bauer GS, Salvatores M, Heusener G. 2001. MEGAPIE, a 1 MW pilot experiment for a
- 1456 liquid metal spallation target. *J. Nucl. Mater.* 296(1–3):17–33
- 1457 123. Wagner W, Dai Y, Glasbrenner H, Aebersold HU. 2007. Materials irradiation facilities at
- 1458 the high-power Swiss proton accelerator complex. *J. Nucl. Mater.* 361(2-3 SPEC.
- 1459 ISS.):274–81
- 1460 124. Kirchner T, Bortoli Y, Cadiou A, Foucher Y, Stutzmann JS, et al. 2003. LiSoR, a liquid metal
- 1461 loop for material investigation under irradiation. *J. Nucl. Mater.* 318(SUPPL):70–83
- 1462 125. Glasbrenner H, Brüttsch R, Dai Y, Gröschel F, Martin M. 2006. Post-irradiation
- 1463 examination on LiSoR 3 experiment. *J. Nucl. Mater.* 356(1–3):247–55
- 1464 126. Glasbrenner H, Gröschel F. 2007. Liquid metal compatibility under irradiation: The LiSoR
- 1465 5 experiment. *J. Nucl. Mater.* 367-370 B(SPEC. ISS.):1590–95
- 1466 127. Glasbrenner H, Dai Y, Gröschel F. 2005. LiSoR irradiation experiments and preliminary
- 1467 post-irradiation examinations. *J. Nucl. Mater.* 343(1–3):267–74
- 1468 128. Dai Y, Glasbrenner H, Boutellier V, Bruetsch R, Jia X, Groeschel F. 2004. Preliminary
- 1469 results of post-irradiation examinations on LiSoR-2 test section. *J. Nucl. Mater.* 335(2
- 1470 SPEC. ISS.):232–38
- 1471 129. Gavrilov S, Lambrecht M, Stergar E, Eremin S, Zhemkov I, et al. 2016. Deliverable D3.9a --
- 1472 PIE of LEXUR II LBE capsules
- 1473 130. Frazer D, Qvist S, Parker S, Krumwiede DL, Caro M, et al. 2016. Degradation of HT9 under
- 1474 simultaneous ion beam irradiation and liquid metal corrosion. *J. Nucl. Mater.* 479:382–89
- 1475 131. Lillard RS, Paciotti M, Tcharnotskaia V. 2004. The influence of proton irradiation on the
- 1476 corrosion of HT-9 during immersion in lead bismuth eutectic. *J. Nucl. Mater.* 335(3):487–
- 1477 92
- 1478 132. Hammer-Rotzler B, Neuhausen J, Boutellier V, Wohlmuther M, Zanini L, et al. 2016.
- 1479 Distribution and surface enrichment of radionuclides in lead-bismuth eutectic from
- 1480 spallation targets. *Eur. Phys. J. Plus 2016 1317.* 131(7):1–18
- 1481 133. Kugler E. 2000. The ISOLDE facility. *Hyperfine Interact.* 129(1–4):23–42
- 1482 134. Dai Y, Henry J, Auger T, Vogt JB, Almazouzi A, et al. 2006. Assessment of the lifetime of
- 1483 the beam window of MEGAPIE target liquid metal container. *J. Nucl. Mater.* 356(1–
- 1484 3):308–20
- 1485 135. Hombourger B, Křepel J, Pautz A. 2019. Breed-and-burn fuel cycle in molten salt reactors.
- 1486 *EPJ Nucl. Sci. Technol.* 5:15
- 1487 136. Forsberg CW, Lam S, Carpenter DM, Whyte DG, Scarlat R, et al. 2017. Tritium Control and
- 1488 Capture in Salt-Cooled Fission and Fusion Reactors: Status, Challenges, and Path Forward.
- 1489 *Nucl. Technol.* 197(2):119–39
- 1490 137. Powers JJ, Wirth BD. 2010. A review of TRISO fuel performance models
- 1491 138. Zheng G, Carpenter D, Ames M, Ostrovsky Y, Kohse G, et al. 2016. Microstructural
- 1492 Characterization of In-reactor Corrosion Tested Hastelloy N and 316 Stainless Steel
- 1493 139. Zhou W, Yang Y, Zheng G, Woller KB, Stahle PW, et al. 2020. Proton irradiation-
- 1494 decelerated intergranular corrosion of Ni-Cr alloys in molten salt. *Nat. Commun.* 11(1):1–

1495 7

1496 140. Ezell NDB, Raiman SS, Kurley JM, McDuffee J. 2020. Neutron Irradiation of Alloy N and
1497 316L Stainless Steel in Contact with a Molten Chloride Salt. *Nucl. Eng. Technol.*

1498 141. Lane JA. 1958. Chapter 12. In *Fluid Fuel Reactors*, p. 591

1499 142. Lane JA. 1958. Behavior of Fission Products. In *Fluid Fuel Reactors*, pp. 588–91

1500 143. McCoy HE, McNabb B. 1972. Intergranular Cracking of INOR-8 in the MSRE -- ORNL-4829.
1501 Oak Ridge, TN (United States)

1502 144. Guo S, Zhang J, Wu W, Zhou W. 2018. Corrosion in the molten fluoride and chloride salts
1503 and materials development for nuclear applications. *Prog. Mater. Sci.* 97:448–87

1504 145. Jia Y, Li Z, Ye X, Liu R, Leng B, et al. 2017. Effect of Cr contents on the diffusion behavior
1505 of Te in Ni-based alloy. *J. Nucl. Mater.* 497:101–6

1506 146. Keiser JR. 1977. Status of tellurium--hastelloy N studies in molten fluoride salts. Oak
1507 Ridge, TN (United States)

1508 147. Delpech S, Cabet C, Slim C, Picard GS. 2010. Molten fluorides for nuclear applications

1509 148. Ignatiev V, Surenkov A. 2013. Alloys compatibility in molten salt fluorides: Kurchatov
1510 Institute related experience. *J. Nucl. Mater.* 441(1–3):592–603

1511 149. Keilholtz GW, Morgan JG, Browning WE. 1959. Effect of Radiation on Corrosion of
1512 Structural Materials by Molten Fluorides. *Nucl. Sci. Eng.* 5(1):15–20

1513 150. Reyes M, Wang P, Was G, Marian J. 2019. Determination of dose rate effects on Zircaloy
1514 oxidation using proton irradiation and oxygen transport modeling. *J. Nucl. Mater.*
1515 523:56–65

1516 151. Nordlund K, Zinkle SJ, Sand AE, Granberg F, Averbach RS, et al. 2018. Primary radiation
1517 damage: A review of current understanding and models. *J. Nucl. Mater.* 512:450–79

1518 152. Aerts A, Lim J, Rosseel K, Marino A, Gonzalez Prieto B, et al. 2018. The conditioning and
1519 chemistry programme for myrrha

1520 153. Yin H, Qiu J, Liu H, Liu W, Wang Y, et al. 2018. Effect of CrF₃ on the corrosion behaviour
1521 of Hastelloy-N and 316L stainless steel alloys in FLiNaK molten salt. *Corros. Sci.* 131:355–
1522 64

1523 154. Cheng H, Li Z, Leng B, Zhang W, Han F, et al. 2015. Intergranular diffusion and
1524 embrittlement of a Ni-16Mo-7Cr alloy in Te vapor environment. *J. Nucl. Mater.* 467:341–
1525 48

1526 155. DeVan JH, DiStefano JR, Eatherly WP, Keiser JR, Klueh RL. 2008. Materials considerations
1527 for molten salt accelerator-based plutonium conversion systems

1528 156. Allen TR, Cole JJ, Kenik EA, Tsai H, Ukai S, et al. 1999. Using fast reactor component
1529 evaluation for pressurized water reactor life extension. *JOM.* 51(10):27–30

1530 157. Zinkle SJ, Busby JT. 2009. Structural materials for fission & fusion energy

1531 158. Bartels D. 2018. Assessment of Corrosion Resistance of Candidate Alloys for Accident
1532 Tolerant Fuel Cladding under Reactor Conditions -- Final Report

1533 159. Wang P, Was GS. 2019. In-situ proton irradiation-corrosion study of ATF candidate alloys
1534 in simulated PWR primary water

1535 160. Zhou W, Woller KB, Zheng G, Stahle PW, Short MP. 2019. A simultaneous
1536 corrosion/irradiation facility for testing molten salt-facing materials. *Nucl. Instruments
1537 Methods Phys. Res. Sect. B Beam Interact. with Mater. Atoms.* 440:54–59

1538 161. Bakai AS. 2008. Combined Effect of Molten Fluoride Salt and Irradiation on Ni-based

- 1539 Alloys
- 1540 162. Toth LM, Felker LK. 1990. Fluorine generation by gamma radiolysis of a fluoride salt
1541 mixture. *Radiat. Eff. Defects Solids*. 112(4):201–10
- 1542 163. Grimes WR. 1964. Reactor Chemistry Division Annual Progress Report, ORNL-3591. Oak
1543 Ridge, TN (United States)
- 1544 164. Akiyama R, Kitaichi M, Fujiwara T, Sawamura S. 1994. Short lived species produced in
1545 pulse irradiated melts of LiF-KF and LiF-NaF-KF eutectic mixtures. *J. Nucl. Sci. Technol.*
1546 31(3):250–52
- 1547 165. Pikaev AK, Makarov IE, Zhukova TN. 1982. Solvated electron in irradiated melts of
1548 alkaline halides. *Radiat. Phys. Chem.* 19(5):377–87
- 1549 166. Baldwin CM, Almeida RM, Mackenzie JD. 1981. Halide glasses. *J. Non. Cryst. Solids.*
1550 43(3):309–44
- 1551 167. Baes CF. 1970. A polymer model for BeF₂ and SiO₂ melts. *J. Solid State Chem.* 1(2):159–
1552 69
- 1553 168. Féron D, Guerre C, Martin F. 2019. Historical review of alloy 600 stress corrosion
1554 cracking: From the “Coriou effect” to the quantitative micro-nano approach
1555

1579 11. Figure Captions

1580 Figure 1:

1581 For liquid nuclear reactor coolants, four main environments can be differentiated: water-, metal-, or salt-cooled,
1582 and a molten salt environment. The classic water-cooled environments have much in common with the Liquid
1583 Metal (LM)-cooled reactor designs: both have evenly spaced fuel rods (yellow) surrounded by cladding that forms
1584 a protective oxide (red), just like other coolant-facing components. LM-cooled reactors, however, are different in
1585 that they are designed to have a fast neutron spectrum and the fuel cladding is typically a stainless steel, as
1586 opposed to Zircaloy found in Light Water Reactors (LWRs). Salt-cooled reactors also use a solid fuel, in this case as
1587 a pebble-bed reactor, similar to gas-cooled designs. The graphitic pebbles contain micro-particles encapsulated
1588 fuel that provide multiple barriers for containment of radioisotopes (orange gradient). Alternatively, in Molten Salt
1589 Reactor (MSR) designs the fuel is dissolved (irregular yellow shapes) within the coolant salt itself. For either salt
1590 reactor environment, the formation of an oxide-based passivating corrosion layer is not expected to occur.

1591

1592 Figure 2:

1593 Energetic particles interact with matter in different ways, depending on their mass, energy, and ionic charge. At
1594 high energies, photons (X-rays and gamma rays) create electron-hole pairs and at low energies, they are simply
1595 absorbed by the material. Light charged particles (e.g., electrons, protons, and alpha particles), primarily interact
1596 with electrons at low energies, but can displace atoms at higher energies, creating vacancy-interstitial pairs. At
1597 high energies, neutrons displace lots of atoms compared to light particles, often in the form of dense damage
1598 cascades, that create many vacancy-interstitial pairs. This defect density decreases with the particle's energy. Swift
1599 heavy ions initially interact with the material by ionizing lattice atoms, but as they lose kinetic energy, they will
1600 create very dense damage cascades.

1601

Deleted:

Deleted:

1624
1625
1626
1627
1628
1629
1630
1631
1632
1633
1634
1635
1636
1637
1638
1639
1640
1641
1642
1643

Figure 3:

Radiation produces a range of effects in crystalline matter, resulting in complex irradiated microstructures. Radiation-induced vacancies and interstitials can either annihilate immediately or migrate through the material and accumulate at secondary defects (e.g., loops, voids, and precipitates). Certain ions can also induce gas production within the material, creating bubbles and volume expansion. Irradiation can also lead to transmutation and subsequently decay, creating a new source of radioactivity and modifying the chemistry of the material. Defect flow can lead to precipitation and elemental segregation. All these processes occur simultaneously in a material and interact with each other, adding to the complexity of the individual processes. Further, all of these effects interact with both the existing and evolving microstructure. Figure inspired by Nordlund et al. (151).

Figure 4:

Schematic illustration of the three different corrosive environments discussed in this review (aqueous, HLM, and molten salt) and some of the most relevant corrosion mechanisms. Materials exposed to aqueous or HLM environments typically develop a protective duplex oxide structure, while no such layer forms in oxygen-poor molten salts where corrosion is inhibited by controlling the salt's chemical redox potential. In all cases corrosion creates an altered base metal that is typically depleted in one or more alloying elements. The ionic nature of water and molten salts also creates a structured double layer in the fluid near the liquid/solid interface. Ongoing corrosion involves the transport and exchange of species between the metal and the fluid through all present layers, which is most efficient along fast diffusion paths, such as grain boundaries and interconnected porosity.

Deleted:

Deleted:

1666
1667
1668
1669
1670
1671
1672
1673
1674
1675
1676
1677
1678
1679
1680
1681
1682
1683
1684
1685

Figure 5:

Illustration (graph from Aerts et al. (152)) of the useful oxygen-content range in LBE. Too much oxygen in the liquid metal leads to the formation of solid lead oxide (black irregular shapes in top schematic on the right), while too little oxygen inhibits the formation of protective oxide layers on materials and subsequently leads to their dissolution by the LBE environment (bottom schematic on the right). These concentrations are temperature-dependent, limiting the operational range of an LBE-cooled reactor.

Figure 6:

Scanning electron microscopy ((a)) and scanning transmission electron microscopy ((c) and (d)) images of oxide layers formed on stainless steel (D9) in flowing LBE (images from (61)). (a) shows a typical duplex oxide structure (illustrated schematically in (b)) where the inner layer can be seen to follow the pre-existing steel grain structure as it grows inward. (c) and (d) show the dense outer layer and a Ni-depleted zone (dark band) between inner and outer layer. (d) shows the segregation of a Ni-rich phase from the Cr-rich oxide, where Ni has diffused out of the grain boundary region and left pores behind.

Figure 7:

Representative examples of corrosion by molten salt. (a) shows examples of oxidative attack, such as grain boundary attack, void formation, and preferential Cr depletion from Yin et al. (153), and (b) shows images of Te embrittlement, a process known to occur in fuel-bearing salts, from Cheng et al. (154) and DeVan et al. (155).

Deleted:

Deleted:

Deleted:

1714
1715
1716
1717
1718
1719
1720
1721
1722
1723
1724
1725
1726
1727
1728
1729
1730
1731
1732
1733
1734
1735
1736
1737
1738

[Figure 8:](#)

Several effects have to be separated in order to study how radiation and corrosion interact: radiation damage in 1) the solid material of interest (e.g., radiation hardening, RIS), 2) the corrosion layer, and 3) the corrosive medium (e.g., radiolysis in water), ignoring the presence of ongoing corrosion, 4) corrosion processes independently of radiation damage, 5) the influence of corrosion products on the chemistry of the corrosive environment, and 6) the influence of the evolving corrosion layer (i.e., impact of its thickness and/or structure on transport rates).

[Figure 9:](#)

The relative abundance of studies using different radiation sources in irradiation-corrosion experiments are shown. Most experiments have used proton beams as a proxy for neutron irradiation in reactors, and about half-as-many employed commercial or test reactors. Most of these reactor studies are significantly older than the proton-based studies. A smaller number of studies report on the corrosion behavior of different materials under heavy ion, electron, and photon irradiation. This is a semiquantitative and non-exhaustive representation based on the literature identified in this review. However, we believe provides a reasonable perspective of the field as a whole, particularly for the current emphasis on proton-based studies.

[Figure 10:](#)

A simplified composite illustration of combined irradiation and corrosion effects discussed separately in [Figure 3](#) and [Figure 4](#). Potential intersections and synergies exist in these coupled extremes, particularly around pre-existing microstructural defects and those newly generated upon corrosion and irradiation. Grain boundaries and heterogeneous interfaces clearly play a critical role in establishing and controlling these linkages as preferential sites for both accelerated transport and enhanced reactivity. This schematic also illustrates that corrosion and irradiation effects are already quite complex on their own, and together they create an even more challenging system. More work in this area is required to fully understand how all the different processes compete and work together, which will be critical for the design and improvement of both materials and coolant chemistries.

Deleted:

Deleted:

Deleted:

Deleted:

Deleted:

1751 **Figure 11:**

1752 Illustration of estimated irradiation exposure rates for LWRs, LBE-cooled reactors, and MSRs (shaded boxes, based

1753 on (25, 156, 157) and an expected reactor lifetime of 60 years) in comparison to reported experimental exposure

1754 rates (dots). Experimental datapoints are limited to studies that reported an exposure estimate, typically from

1755 proton irradiation. Most experimental studies employ accelerated testing conditions with dose rates that are much

1756 higher than expected in-reactor. Datapoints: 1: (114), 2: (112), 3: (106), 4: (158), 5: (159), 6: (156), 7: (120), 8:

1757 (128), 9: (127), 10: (126), 11: (115), 12: (139, 160), 13: (161)

1764 12. Figures

1765 Figure 1:

Deleted:

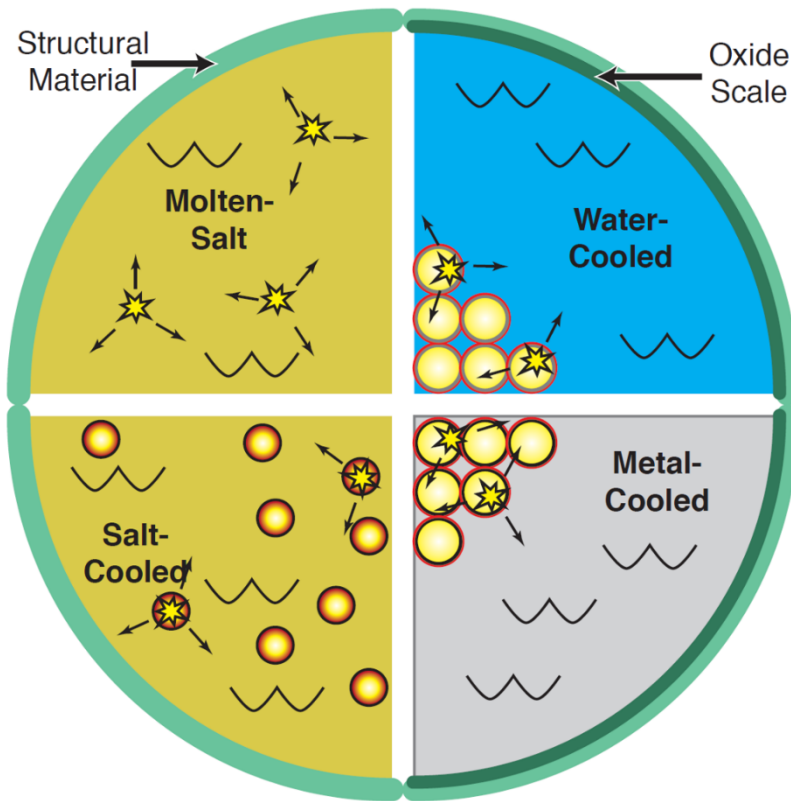
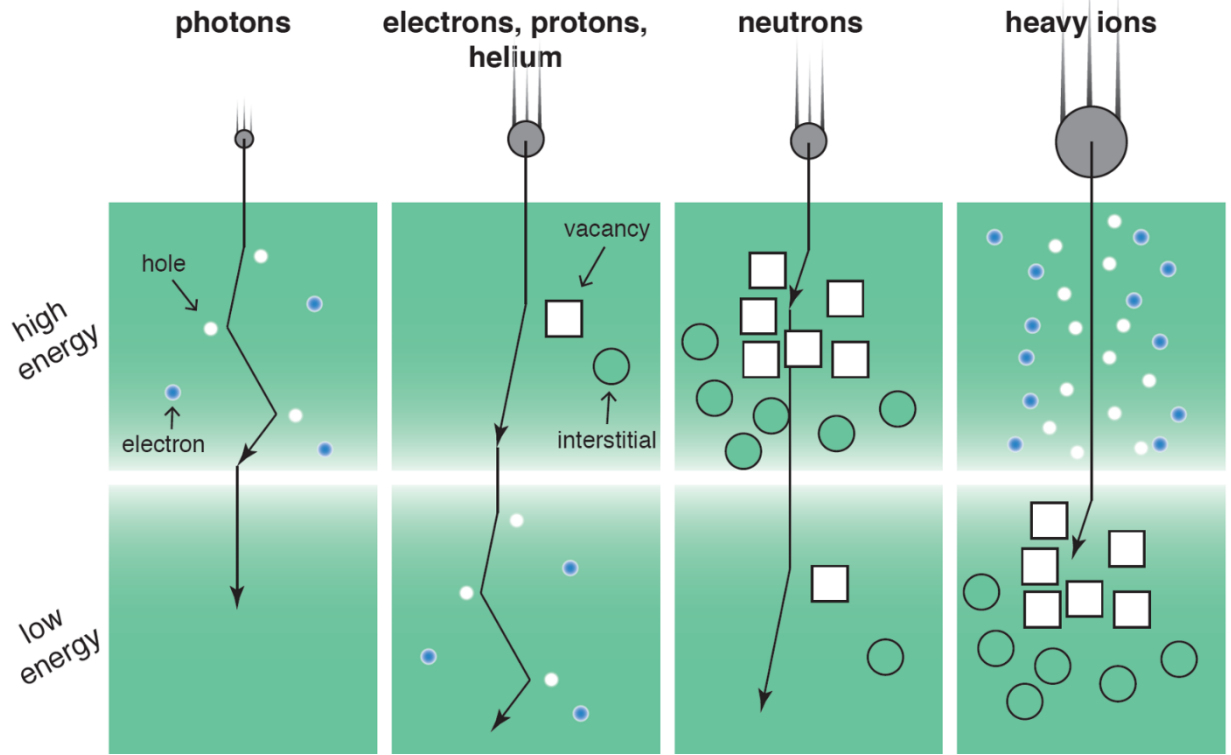


Figure 1

1766

1767

1768

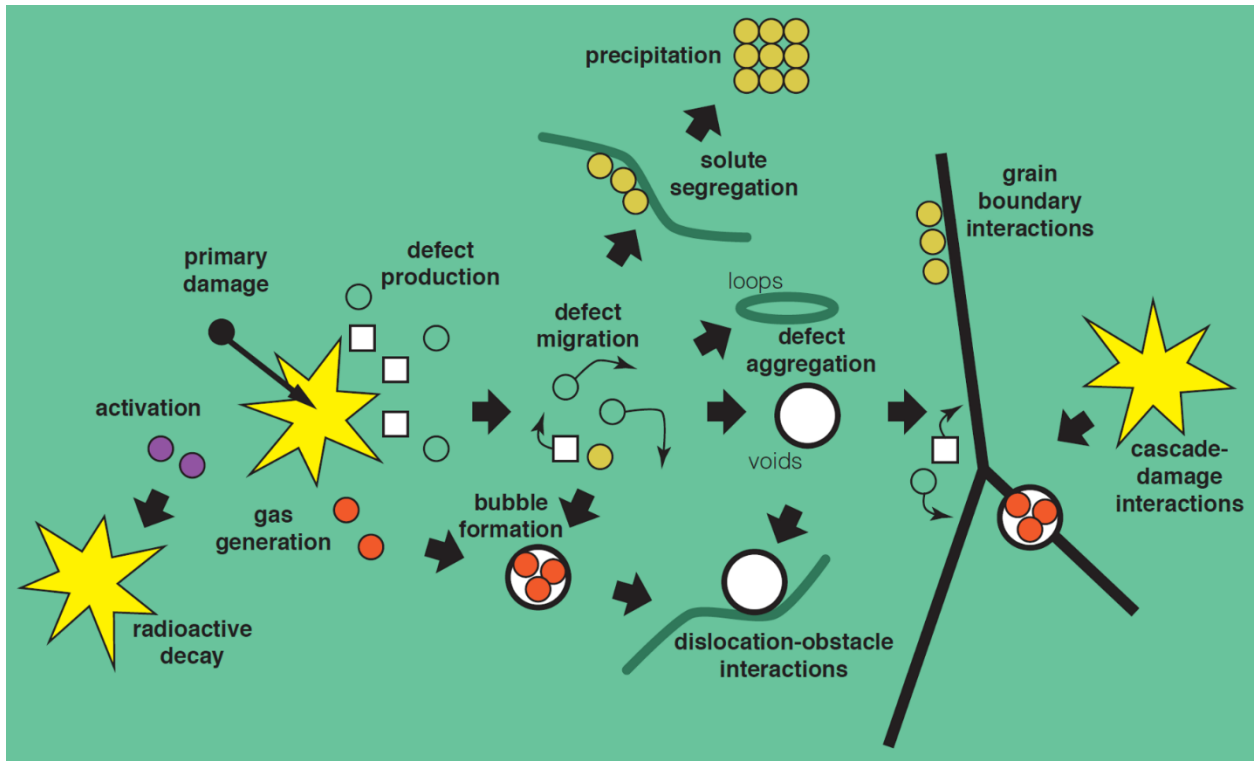


1775

1776

1777

Figure 2

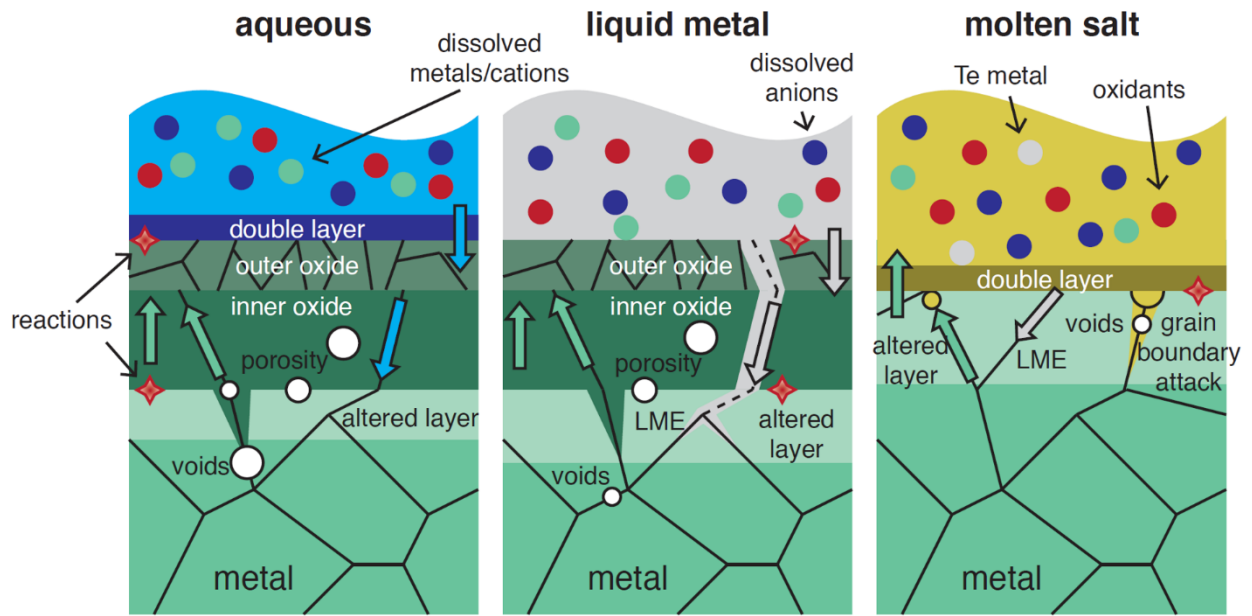


1784

1785

1786

Figure 3



1793

1794

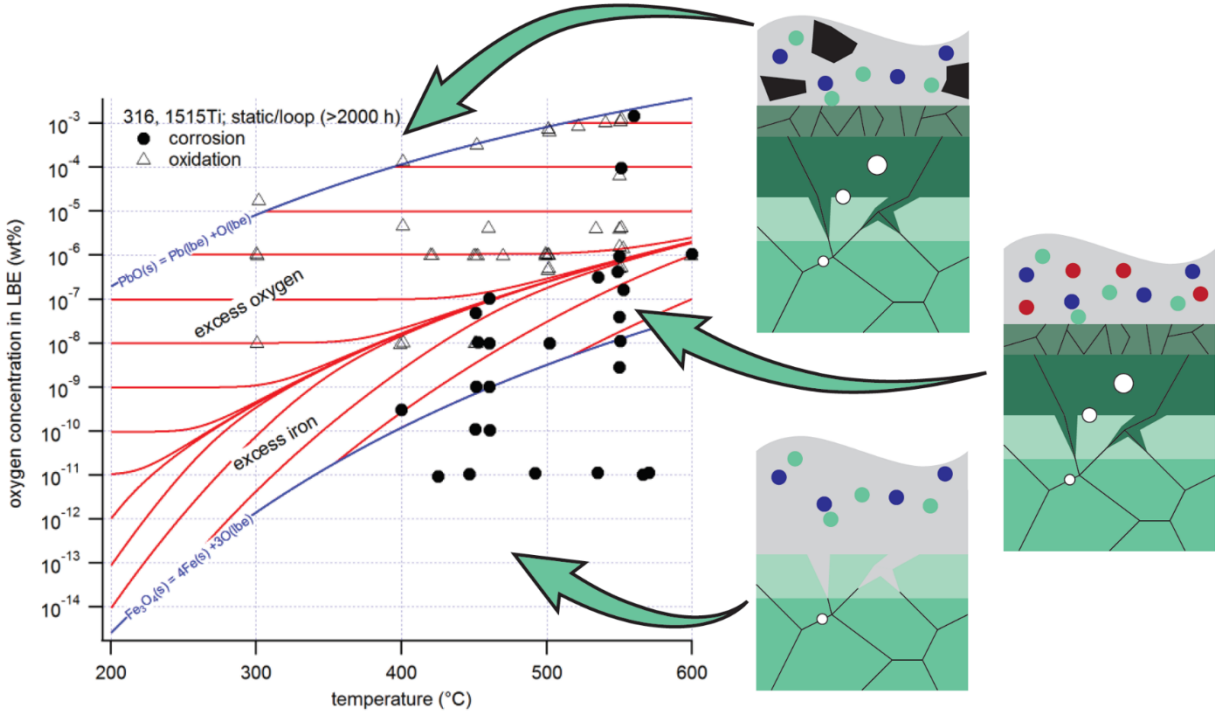
1795

Figure 4

1801

Figure 5:

Deleted:



1802

1803

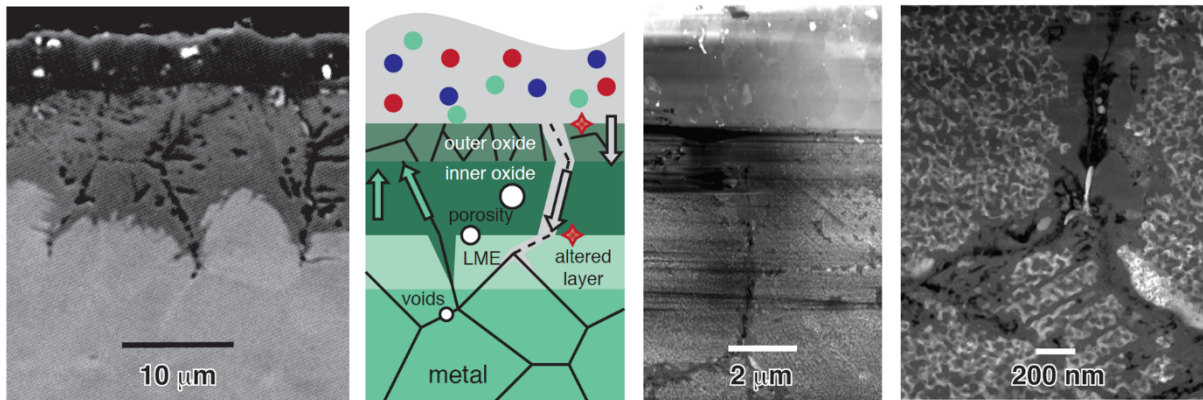
1804

Figure 5

1810

Figure 6:

Deleted:



1811

1812

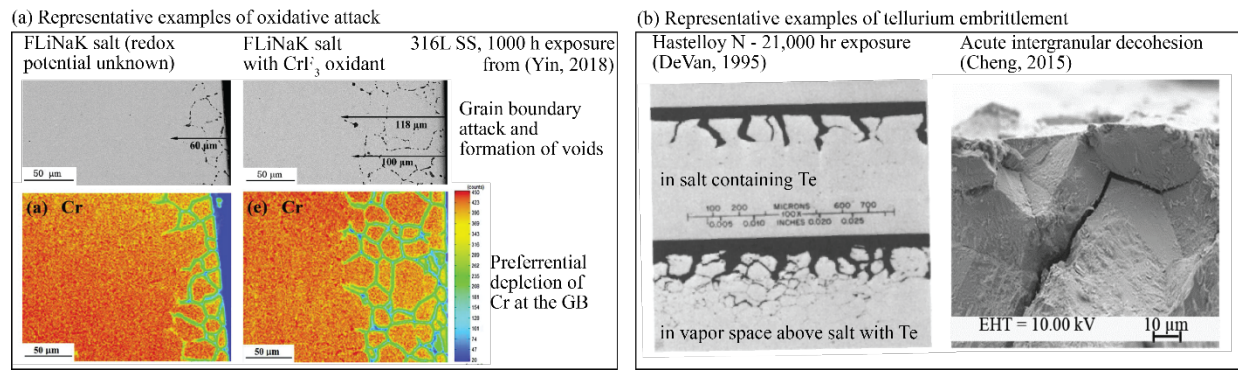
1813

Figure 6

1819

Figure 7:

Deleted:



1820

1821

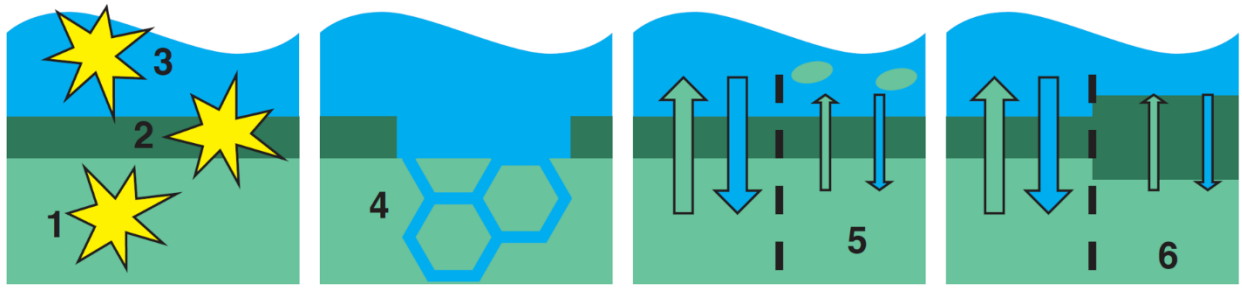
1822

Figure 7

1828

Figure 8;

Deleted:



1829

1830

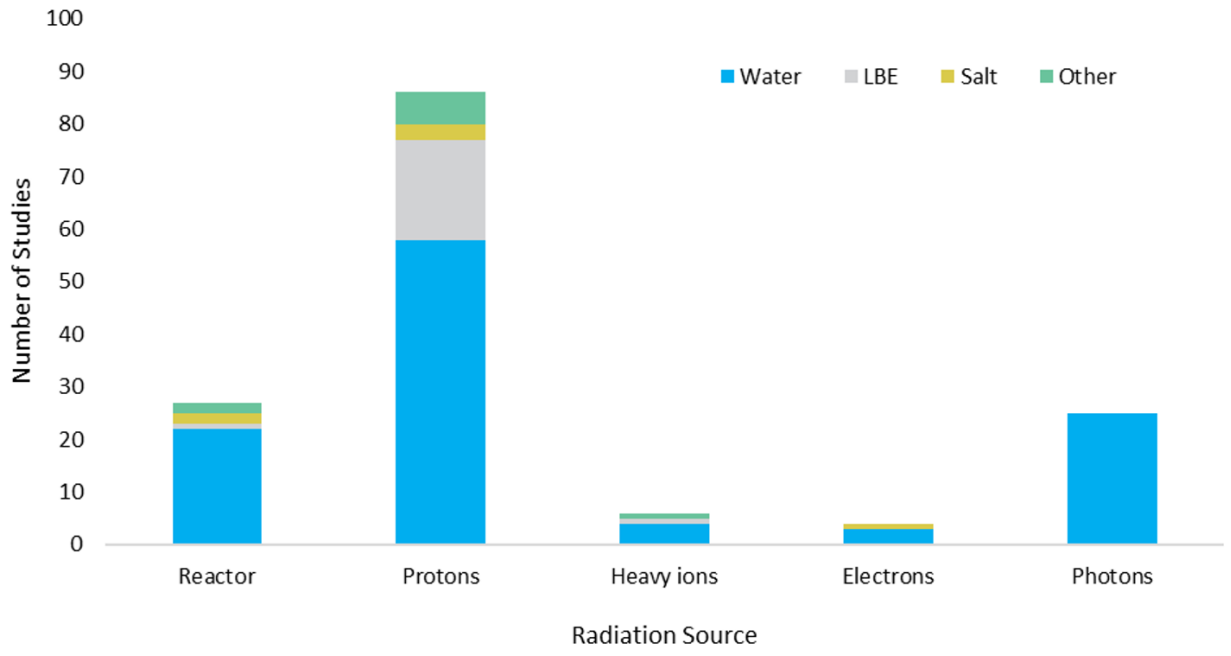
1831

Figure 8

1837

Figure 9:

Deleted:



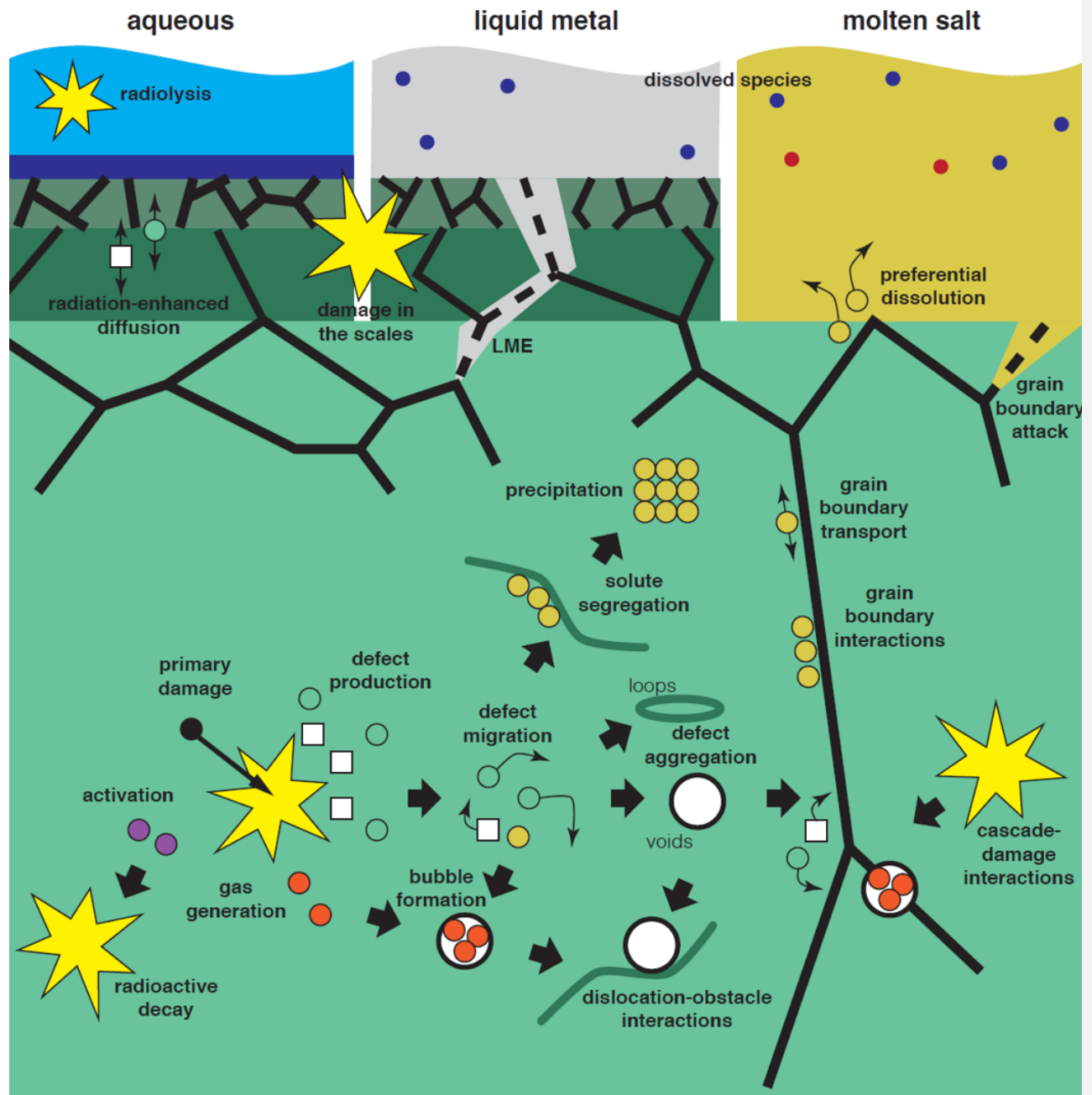
1838

1839

1840

Figure 9

Figure 10:



1847

1848

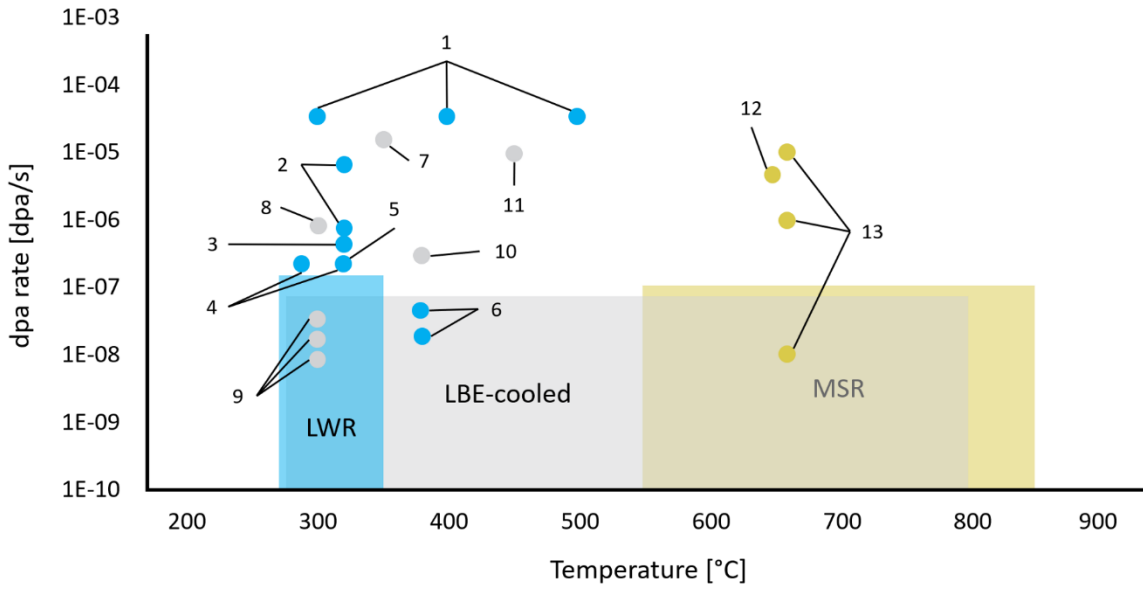
1849

Figure 10

1855

Figure 11;

Deleted:



1856

1857

1858

Figure 11

1860 13. Terms and Definitions

1861 LBE: a possible coolant for fast reactors (55.5 wt% Bi, 45.5 wt% Pb)

1862 LWRs: water-cooled reactors with light water as coolant and moderator, as opposed to heavy
1863 water reactors that use deuterium oxide

1864 Radiolysis: the breaking of molecular bonds or modification of valence states by ionizing
1865 radiation

1866 HLM: high-Z metal with melting points higher than traditional liquid metals, i.e., significantly
1867 higher than room temperature

1868 Transmutation products: elements produced in solid and liquid reactor components as the
1869 result of nuclear reactions other than fission

1870 FPs: elements produced by fission with masses unequal to parent nucleus mass (centered
1871 around ~95 and ~140 atomic mass units)

1872 RED and RIS: mechanisms based on radiation-induced defects that exacerbate species
1873 redistribution at temperatures too low for significant thermal diffusion

1874 dpa: unit that captures radiation exposure conditions of a material, not the remaining damage,
1875 which is a common misconception

1876 F/M: often called 9-12% Cr steels that were developed to have favorable mechanical properties
1877 at high temperatures

1878 CRA: designed to provide long-term corrosion resistance to uniform corrosion, but may still be
1879 susceptible to other corrosion types

1880 LME: a process that can lead to a rapid loss of ductility in metals via intrusion of other metallic
1881 species

1882 SCC: corrosion mode characterized by crack propagation of susceptible stressed materials in an
1883 unfavorable environment; can be exacerbated by radiation (IASCC)

1884 Redox potential: defines the chemical equilibrium of the products of oxidizing corrosion and the
1885 propensity of an environment to oxidize materials

1886 Redox reaction: a species increases in valence (oxidizes) and another species (oxidant causing
1887 corrosion) decreases in valence (reduces)

1888 Carburization: transport of C into metal alloys, leading to degradation of their mechanical
1889 properties

1890 FLiBe: fluoride salt mixture, $2\text{LiF}-\text{BeF}_2$, employed as in-reactor nuclear fuel solvent or coolant
1891

1892 14. Reference Annotations

1893 (25) In-depth summary of ion beam applications and limitations for long-term reactor damage

1894 simulation

1895 (33) Seminal paper on the chemistry and thermodynamics of molten salt reactor fuels

1896 (42) Extensive discussion of experimental evidence for potential Zircaloy irradiation-corrosion

1897 mechanisms

1898 (78) Review of corrosion phenomena and corrosion experience in molten salts

1899 (79) Summary of four years of operating experience with the MSRE

1900 (93) Summary of the effects of hydrogen on Zircaloy properties

1901 (94) Introduction to IASCC in nuclear materials in water

1902 (121) Comprehensive presentation of LBE properties including detailed discussion of

1903 recommended values for each property

1904

1905 15. Sidebars

1906 Considerations in Reactor Design

1907 Modern nuclear reactors seek to depart from conventional reactor designs for a broad range of
1908 reasons, including decreasing capital cost, lowering time of deployment to the grid, providing a
1909 more diverse set of energy products (e.g. hydrogen production, power peaking, off-grid power,
1910 process heat) and providing alternative options for the lifecycle of the nuclear fuel. Energy
1911 conversion efficiency is generally improved by moving to coolants that allow for operation at
1912 higher temperatures, which introduces new mechanical and corrosion challenges for structural
1913 materials. The new coolants in modern reactor designs also enable simpler designs, greater
1914 inherent safety, and afford more options for passive safety to complement the active safety
1915 systems. Lastly, reactors can operate in the thermal neutron spectrum (neutron energies
1916 around 0.025 eV), which utilize a moderator (e.g., water, graphite) to reduce the kinetic energy
1917 of fission neutrons; alternatively, reactors can operate in the fast neutron spectrum (> 1 MeV),
1918 requiring materials that can withstand the harsher irradiation conditions (higher fast neutron
1919 spectrum), but enabling better fuel utilization and lowering the long-term waste burden. All
1920 these and more requirements lead to several interesting tradeoff considerations for the next
1921 generation of nuclear reactors.

1922

1923 Radiolysis in Molten Salt

1924 Molten salts are ionic liquids, consisting of dissociated anions and cations. An argument has
1925 been made that radiolysis is not of relevance in molten salts. Studies of the vapor species above
1926 irradiated molten fluoride salt observed no differences upon irradiation; by contrast, $F_2(g)$
1927 evolution can occur upon irradiation of solid fluoride salt (162, 163). This argument is
1928 challenged by the observation that irradiation can cause halide anions (e.g. F^-) to dissociate into
1929 solvated electrons (e^-) and solvated neutral species (F) that form molecular radical ions (F_2^-).
1930 The diffusivities and recombination kinetics are high in high temperature ionic liquids and these
1931 species do not persist beyond 1-2 μs for solvated electrons and 10s μs for the radical ions (164,
1932 165). Thus, the expected concentration of radiolysis products is low. What has not yet been
1933 investigated is the effect of radiolysis on the short-range order in the molten salts. In acidic
1934 salts, complex anions (and even complex cations) can form; the bonds within the complex ions
1935 can be of an ionic or covalent nature (166, 167). It is unknown if radiolysis disrupts the structure
1936 of these complex ions, thus impacting the acidity of the melts.
1937

1938 Leak-Before-Break

1939 An important engineering criterion for structural components in nuclear reactors is that they
1940 exhibit favorable failure characteristics. In the context of corrosion, it is of paramount
1941 importance that components exhibit signs of impending failure that can be readily detected
1942 prior to catastrophic component failure. This philosophy is embodied by the “leak before
1943 break” concept, wherein a small coolant leak may indicate component degradation well before
1944 a catastrophic failure event. A swift response in the form of component identification,
1945 anticipation and management of damage accumulation, accomplished through an appropriate
1946 component inspection schedule by non-destructive evaluation methods, is vital for accident
1947 prevention. These schedules and methods are well established in the current LWR fleet, but
1948 have yet to be as thoroughly developed for next-generation designs where the underlying
1949 science of corrosion and material degradation and failure have yet to be understood.
1950 Regardless of the coolant, material, and environment combination, components will inevitably
1951 degrade and fail in these aggressive conditions and it is vital for the safe and economical
1952 operation of these plants that these failures can be proactively detected and mitigated.
1953

1954 A Quick Note About Math

1955 It is commonplace to consider the growth of oxide scales to be time dependent and
1956 proportional to t^n with time t and n ranging from 1 (linear) to 0.25. These highly varied
1957 exponents result in very different behaviors across the lifetime of a nuclear reactor. After 60
1958 years of service, a material that corrodes at a linear rate will have oxidized ~8 times as much as
1959 a material corroding with $n = 0.5$. Compared to $n = 0.33$ and $n = 0.25$, the performance is even
1960 worse with oxidation depths that are more than 15 and 21 times higher, respectively.
1961 Depending on the thickness of the component or how much heat it needs to transfer, larger
1962 exponents may be unacceptable. In practice, various environmental conditions can shift a
1963 material's response into different corrosion rate regimes during its service life. However, it is
1964 most critical that so-called "runaway" corrosion conditions be avoided, where corrosion
1965 accelerates continuously ($n > 1$ or exponential growth). Both materials selection and coolant
1966 chemistry control are key factors that control corrosion mode and rate, making the study of
1967 their interactions central to reactor safety.
1968

1969 Failure Mechanisms in HLM Systems

1970 The formation of intermetallics in the liquid due to the presence of dissolved species from
1971 corrosion provides concentration gradients that continuously drive corrosion, so does the heat
1972 gradient. The removal of elements on the hot side leads to a reduced wall thickness, which
1973 increases the potential for pipe bursts, while precipitation can lead to pipe clogging. This can be
1974 mitigated by reducing the driving force for dissolution or by adding diffusion barriers to reduce
1975 the dissolution rate by controlling HLM chemistry. While corrosion processes can lead to system
1976 failure, it is important to note that this is a slow process and the goal is typically to slow it down
1977 beyond the lifetime of a plant, not to prevent it completely. In contrast, LME, where the
1978 presence of HLMs drastically reduces a component's ductility, typically occurs much more
1979 rapidly, potentially violating the aforementioned "leak before break" concept. Therefore,
1980 chemistry control and careful alloy design is aimed at preventing LME and the associated rapid
1981 crack propagation completely.

1982

1983 Lesson Learned in Materials Design

1984 Materials for early nuclear reactors were chosen based on a thoughtful but imperfect process
1985 considering factors such as temperature, mechanical properties, corrosion, and nuclear
1986 properties, e.g., neutron cross section. Many selections had to be revised over time after
1987 numerous lessons were learned. Consider SCC. Initially, reactors were thought to be immune to
1988 cracking given CRAs, high purity water free of Cl⁻, and controlled stresses. However, soon it was
1989 discovered that CRAs in hot high purity water in submarine reactors experienced SCC, often in
1990 welded stainless steel components and steam generator tubes. The former was solved by
1991 avoiding sensitization. In commercial plants, alloy 600 was selected for steam generators based
1992 on good oxidation resistance (15% Cr) and good SCC resistance (> 40% Ni). However, this
1993 alleged “safe” composition was based on short-term testing in a high Cl⁻ environment unlike
1994 that in PWRs. In 1959, Henri Coriou first found that plastically deformed alloy 600 with 75% Ni
1995 was susceptible to IGSCC in hot water, a widely criticized finding (168). It was not until around
1996 1980, that Coriou’s observations were well accepted. In response, alloy 600 was replaced by
1997 other more highly alloyed materials, an expensive process that took several decades to
1998 complete.
1999

2000 Windows of Susceptibility

2001 It is widely accepted that reactor materials are not immune to corrosion. Most materials
2002 corrosion problems require a susceptible metallurgical condition and a specific environment
2003 that enables various undesired types and rates of corrosion. Long reactor component lifetimes
2004 with high reliability require studies where materials are exposed to a range of conditions with
2005 low corrosion rates. The undesirable degradation of CRAs occurs in certain “windows” of
2006 susceptibility. Unfortunately, there is uncertainty over whether short-term lab tests can
2007 accurately define such windows. The longer the service lifetimes (up to decades) of nuclear
2008 materials in comparison to lab-scale test times (~minutes to years), the greater the risk that the
2009 windows of susceptibility will remain uncertain. For instance, short-term IGSCC susceptibility,
2010 where initiation, propagation and failure occur quickly, easily reveals the most susceptible
2011 conditions in a short-term test at the lab scale. Long-term susceptibility under conditions more
2012 relevant to service conditions are sometimes unobservable in short term tests, but remain
2013 pertinent to reactors with extended lifetimes. As more sensitive tests are employed and more
2014 realistic conditions are simulated, the bounds of the observable susceptibility windows may
2015 change.

2016